Oceanic core complex development at the ultraslow spreading Mid-Cayman Spreading Center

N. W. Hayman, N. R. Grindlay, M. R. Perfit, P. Mann, Sylvie Leroy, B. Mercier de Lépinay

Geochemistry Geophysics Geosystems G3

Article
Volume 12, Number 3
15 March 2011
Q0AG02, doi:10.1029/2010GC003240
ISSN: 1525-2027

Published by AGU and the Geochemical Society

Oceanic core complex development at the ultraslow spreading Mid-Cayman Spreading Center

Nicholas W. Hayman
Institute for Geophysics, Jackson School of Geosciences, University of Texas at Austin, J. J. Pickle Research Campus, 10100 Burnet Road, Building 196, Austin, Texas 78758, USA (hayman@ig.utexas.edu)

Nancy R. Grindlay
Center for Marine Science, University of North Carolina at Wilmington, 5600 Marvin Moss Lane, Wilmington, North Carolina 28409, USA

Michael R. Perfit
Department of Geological Sciences, University of Florida, PO Box 112120, Gainesville, Florida 32611, USA

Paul Mann
Institute for Geophysics, Jackson School of Geosciences, University of Texas at Austin, J. J. Pickle Research Campus, 10100 Burnet Road, Building 196, Austin, Texas 78758, USA

Sylvie Leroy
ISTEP UPMC-UMR 7193, 4 place Jussieu, F-75252 Paris, France

Bernard Mercier de Lépinay
Géosciences Azur, UMR CNRS 6526, 250 rue Albert Einstein, bâtiment 4, F-06560 Valbonne, France

[1] Roughly a third of the global mid-ocean ridge system spreads at <20 mm/yr (full rate) with predicted low crustal thicknesses, great axial depths, end-member basalt compositions, and prominent axial faults. These predictions are here further investigated along the ultraslow (15–17 mm/yr) Mid-Cayman Spreading Center (MCSC) through a compilation of both previously published and unpublished data. The MCSC sits along the Caribbean-North American plate boundary and is one of the world's deepest (>6 km) spreading centers, and thought to accrete some of the thinnest (~3 km) crust. The MCSC generates end-member mid-ocean ridge basalt compositions and hosts recently discovered hydrothermal vents. Multibeam bathymetric data reveal that axial depth varies along the MCSC with intraridge rift walls defined by kilometer-scale escarpments and massifs. Dredging and near-bottom work has imaged and sampled predominantly basaltic lavas from the greatest axial depths and ~15% peridotite surrounded by gabbroic rocks from the prominent massifs. The gabbroic rocks exhibit wide compositional variation (troctolites to ferrogabbros) and in many places contain high-temperature (amphibolite to granulite facies) shear zones. Gabbroic compositions primarily reflect the accumulation of near-liquidus phases that crystallized from a range of basaltic melts, as well as from interactions with interstitial melts in a subaxial mush zone. Magnetization variations inverted from aeromagnetic data are consistent with a discontinuous distribution of basaltic lavas and structurally asymmetric spreading. These observations support an oceanic core complex model for MCSC seafloor spreading, potentially making it a type example of ultraslow seafloor spreading through mush zone and detachment fault crustal processes.

Components: 12,200 words, 10 figures.

Keywords: Cayman; ultraslow; oceanic core complex; detachment; gabbro; hydrothermal.

Index Terms: 3035 Marine Geology and Geophysics: Midocean ridge processes.

Received 28 May 2010; **Revised** 11 January 2011; **Accepted** 26 January 2011; **Published** 15 March 2011.

Hayman, N. W., N. R. Grindlay, M. R. Perfit, P. Mann, S. Leroy, and B. M. de Lépinay (2011), Oceanic core complex development at the ultraslow spreading Mid-Cayman Spreading Center, *Geochem. Geophys. Geosyst.*, *12*, Q0AG02, doi:10.1029/2010GC003240.

Theme: Oceanic Detachment Faults
Guest Editors: J. P. Canales, M. Cheadle, J. Escartín, G. Fruh-Green, and B. John

1. Introduction

[2] Mid-ocean ridge (MOR) spreading centers are intriguing tectonic environments because of rich feedbacks between magmatism, volcanism, faulting, and hydrothermal fluid flow. These feedbacks ultimately control first-order MOR properties such as crustal thickness. Though a general and clear-cut relationship between spreading rate and crustal thickness is controversial [e.g., *Chen*, 1992], a prevailing MOR model predicts a wide upper mantle thermal boundary layer at ultraslow spreading rates (<20 mm/yr, full rate), resulting in a low melt supply and thinner crust [*Reid and Jackson*, 1981; *White et al.*, 2001]. Several MOR characteristics are thought to result from such crustal accretion conditions, including great axial depth, global end-member major element basalt composition, and a low density of hydrothermal vents along a given ridge length [*Klein and Langmuir*, 1987; *Baker et al.*, 1996]. Ultraslow spreading centers can even host truly amagmatic ridge segments dominated by suites of mantle rocks [*Dick et al.*, 2003]. Yet, first-order models do not explain why several ultraslow ridge segments have locally abundant magmatism and hydrothermal activity [*Okino et al.*, 2002; *Michael et al.*, 2003; *Baker and German*, 2004]. The surprising observation of magmatism and hydrothermal activity on some ultraslow spreading centers has implications for all spreading rates, and especially for linkages between melt supply and crustal structure [e.g., *Baran et al.*, 2009].

[3] A recent conceptual model captures much of the heterogeneity of ultraslow spreading centers [*Cannat et al.*, 2006]. The two end-members of this model are (1) symmetric spreading of faulted, magmatic crust and (2) exhumation of smooth seafloor that is dominated by mantle rocks. Between these two styles of seafloor spreading, domal massifs rise kilometers above the adjacent intraridge rifts. The massifs are called oceanic core complexes (OCCs) [e.g., *Karson*, 1999] and include both exhumed mantle peridotite and gabbroic rocks [*Tucholke et al.*, 1998; *Ildefonse et al.*, 2007]. Studies of OCCs along the Southwest Indian Ridge (SWIR) and the Mid-Atlantic Ridge (MAR) focus on characteristic bathymetric patterns of curviplanar surfaces [*Cann et al.*, 1997; *Smith et al.*, 2006], distinctive patterns of microseismicity [*de Martin et al.*, 2007], and seafloor outcrops of deformed and altered rocks [*Escartín et al.*, 2003; *Karson et al.*, 2006]. Additional geochronologic [*John et al.*, 2004; *Grimes et al.*, 2008] and paleomagnetic data [*Garcés and Gee*, 2007; *Morris et al.*, 2009] further show that the detachment faults helped exhume deeper crustal and upper mantle footwalls and stripped away overlying basaltic hanging walls. In these settings, the OCC's footwalls likely initially developed in crystal-melt mush zones that froze before or during their exhumation [*Dick*, 1989; *Lissenberg and Dick*, 2008; *Suhr et al.*, 2008a, 2008b; *Drouin et al.*, 2010; *Warren and Shimizu*, 2010; *Dick et al.*, 2010]. In turn, the final phases of exhumation appear to coincide with hydrothermal alteration including serpentinization of mantle peridotite [*MacLeod et al.*, 2009]. Altogether, these observations motivate numerical models of seafloor spreading that dynamically link spreading rate, magmatism, and faulting [*Buck et al.*, 2005; *Behn and Ito*, 2008; *Ito and Behn*, 2008; *Olive et al.*, 2010].

[4] The Mid-Cayman Spreading Center (MCSC) offers an arguably unique opportunity to evaluate the applicability of the OCC model to ultraslow spreading processes. Though in an apparently "anomalous"

setting surrounding by continental and arc crust of the Caribbean and North American plates, Cayman trough basalts are devoid of any subducted-slab geochemical signature [*Perfit*, 1977; *Perfit and Heezen*, 1978; *CAYTROUGH*, 1979; *Elthon et al.*, 1995] and produce seafloor magnetic anomalies that record ~15–20 mm/yr spreading rates from mid-Eocene time [*Rosencrantz et al.*, 1988; *Leroy et al.*, 2000]. A widely cited end-member for mid-ocean ridge basalt (MORB) geochemistry and great axial depth (>6 km) [*Klein and Langmuir*, 1987], existing geophysical data further suggest that the Cayman trough contains some of the thinnest (~3 km) oceanic crust in the world [*Ewing et al.*, 1960; *Bowin*, 1968; *ten Brink et al.*, 2002].

[5] The MCSC is also an important and accessible study area for ultraslow spreading hydrothermal systems. Variably deformed and hydrothermally altered crust, and recently discovered hydrothermal venting characterize the MCSC [*Ito and Anderson*, 1983; *German et al.*, 2010; *Murton et al.*, 2010]. A black smoker vent system in the axial region of the MCSC may reach exceptionally high temperatures because of higher pressures imposed by the water column. Furthermore, the MCSC may host ecosystems that have been isolated from the East Pacific Rise (EPR) or Mid-Atlantic Ridge (MAR) vent systems, important for biologists trying to resolve the evolution of biogeographical provinces [*Tyler et al.*, 2002; *Van Dover et al.*, 2002]. An off-axis sulfide/sulfate mound vents relatively clear, moderate-temperature fluids at a high flux, evidence for either an unusually wide axial hydrothermal system or, alternatively, for off-axis magmatism. Understanding the geological and geophysical structure of the MCSC is a key part of understanding these hydrothermal vent fields, and in turn the hydrothermal system dynamics will affect the geodynamics of the spreading center.

[6] Here we present previously unpublished data from the MCSC, including (1) bathymetric data and remotely operated vehicle (ROV) samples collected on the 2002 CAYVIC R/V *L'Atalante* research cruise [*Ruellan et al.*, 2003], (2) aeromagnetic data collected in 1991 [*Rosencrantz*, 1995], and (3) petrologic and geochemical results from previously dredged and Alvin-collected samples [*Perez-Suarez*, 2001]. When synthesized with previously published results, these data bring an OCC model for the MCSC into focus. We explore this model and its significance both for the tectonic and geodynamic history of the Cayman trough, and for its implications for ultraslow spreading-center processes worldwide.

2. History of Mid-Cayman Spreading Center Studies

[7] The MCSC was first recognized during early studies of the North American-Caribbean plate boundary [*Molnar and Sykes*, 1969], and its <20 mm/yr spreading rate successfully constrained the Caribbean plate kinematics [*Jordan*, 1975]. The recognition of seafloor magnetic anomalies [*Holcombe and Sharman*, 1983], sampling of ocean crustal rocks [*Perfit*, 1977; *Perfit and Heezen*, 1978; *CAYTROUGH*, 1979; *Stroup and Fox*, 1981], and normal-fault earthquakes (Figure 1) collectively reinforced the finding of seafloor spreading in the MCSC.

[8] The kinematics of MCSC spreading are best understood in a North American reference frame. In this reference frame, the northwestern margin of the Cayman trough is an inactive fracture zone, and the Oriente and Swan Island transforms (zones) to the northeast and southwest, respectively, are left lateral systems, as illustrated by earthquake distributions and focal mechanisms (Figure 1). The southeastern margin of the Cayman trough is more difficult to interpret as an inactive fracture zone. Though large earthquakes have not been recorded on the submarine escarpment of the Cayman trough west of Jamaica (Figure 1), young fault scarps and continuity with the active Walton (Enriquillo-Plantain Garden) fault in Jamaica and Hispañola attest to activity there [*Rosencrantz and Mann*, 1991; *Dixon et al.*, 1998]. However, the Walton fault system is left lateral and has a slip rate of ~7 mm/yr [*DeMets et al.*, 2007]. The prevailing explanation for the Walton fault kinematics is that on eastern side of the MCSC the Gonave microplate moves at a slightly different rate and direction than the adjacent Caribbean plate [*DeMets and Wiggins-Grandison*, 2007]. Caribbean-North American plate motion varies from ~18 to ~22 mm/yr depending on location and data quality [*DeMets et al.*, 2007], and MCSC spreading rate estimates range from ~15 to ~20 mm/yr based on differing interpretations of magnetic anomaly data [*Macdonald and Holcombe*, 1978; *Rosencrantz et al.*, 1988; *Leroy et al.*, 2000]. Our interpretation of previously unpublished Cayman trough aeromagnetic data, presented in section 4, suggests that the MCSC spreads at ~15 mm/yr. If the Caribbean plate moves eastward

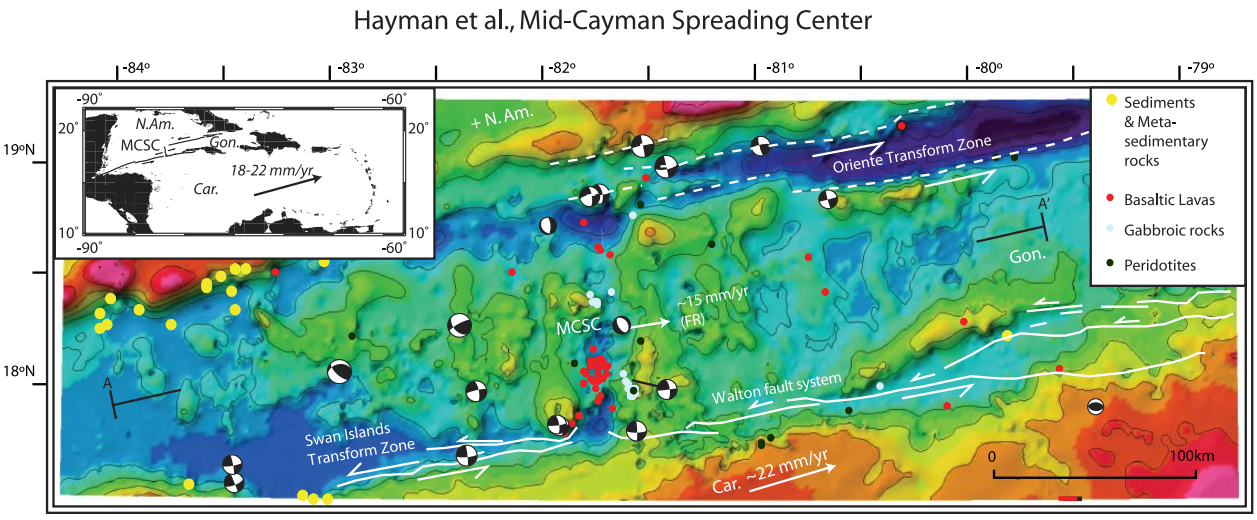

Figure 1. (inset) Location of the Mid-Cayman Spreading Center (MCSC): Caribbean (Car.)–North American (N.Am.) plate vector is representative of the range determined by *DeMets et al.* [2007]. The Gonave microplate (Gon.) is defined geodetically by motion of Jamaica relative to the Caribbean plate [*DeMets and Wiggins-Grandison*, 2007]. Map of the Cayman trough: bathymetry is from http://www.geomapapp.org and fault traces (white lines) are from *Rosencrantz and Mann* [1991]. Earthquake focal mechanisms are from the Harvard Centroid Moment Tensors for Mw > 5. Dots are dredge locations colored for different rock types (see key). See text for details.

at ~22 mm/yr with respect to the North American plate, then this is consistent with a ~7 mm/yr left-lateral slip across the Walton fault system in the vicinity of the MCSC. We note, however, that the magnetic anomalies only record the geological spreading rate, there could be a slip rate gradient along the Walton fault system, and the geodetic solution may improve with continued geodetic monitoring.

[9] Crustal provinces that surround the Cayman trough include: Caribbean arc and associated ophiolitic fragments, volcanics of the Caribbean Large Igneous Province (CLIP), and older Jurassic to pre-Jurassic age Mayan and Chortis continental crustal blocks [*Perfit and Heezen*, 1978; *Mann*, 1999]. The Chortis block and the CLIP were positioned adjacent to the Great Caribbean arc by late Campanian time (ca. 80–72 Ma) [*Mann*, 2007]. Pre-Eocene age crustal extension within the Caribbean plate has not been recognized [*Leroy et al.*, 1996].

[10] The earliest possible initiation of MCSC seafloor spreading is 49–56 Ma based on the proposed presence of magnetic anomaly 22 [*Leroy et al.*, 2000]. Previous workers identified magnetic anomaly 20 (~45 Ma) and determined similar ages of initial seafloor spreading via subsidence and cooling models [*Rosencrantz et al.*, 1988], and geologic relationships between the Cayman and Nicaraguan (morphological) rises [*Perfit and Heezen*, 1978; *Leroy et al.*, 1996]. An alternative hypothesis is that older parts (~250–430 km off axis) of the Cayman trough are, in fact, underlain by extended arc and/or continental crust, perhaps with areas of pervasively serpentinized mantle [*ten Brink et al.*, 2002]. This latter hypothesis derives from an analysis of gravity data that also led *ten Brink et al.* [2002] to predict crustal thickness changes at ~10 Ma, and a less well-defined and more asymmetric crustal thickness change at ~20 Ma (Figure 2). These variations are superposed on a broader asymmetric structure of the Cayman trough determined in early geophysical studies wherein the east side of the MCSC is characterized by overall thinner crust, thinner seismic velocity layer 2, lower heat flow, and a slightly deeper and smoother bathymetric profile (Figure 2) [*Erickson et al.*, 1972; *Jacobs et al.*, 1989].

3. Bathymetric and Geologic Structure of the Mid-Cayman Spreading Center

[11] The structure of the MCSC is greatly clarified by previously unpublished bathymetric data collected on the 2002 French CAYVIC cruise on the R/V *L'Atalante*, which also deployed the remotely operated vehicle (ROV) Victor on three dives [*Ruellan et al.*, 2003]. In Figure 3 we present a color-shaded map of the MCSC bathymetry overlain with both the 2002 dive tracks and also the late

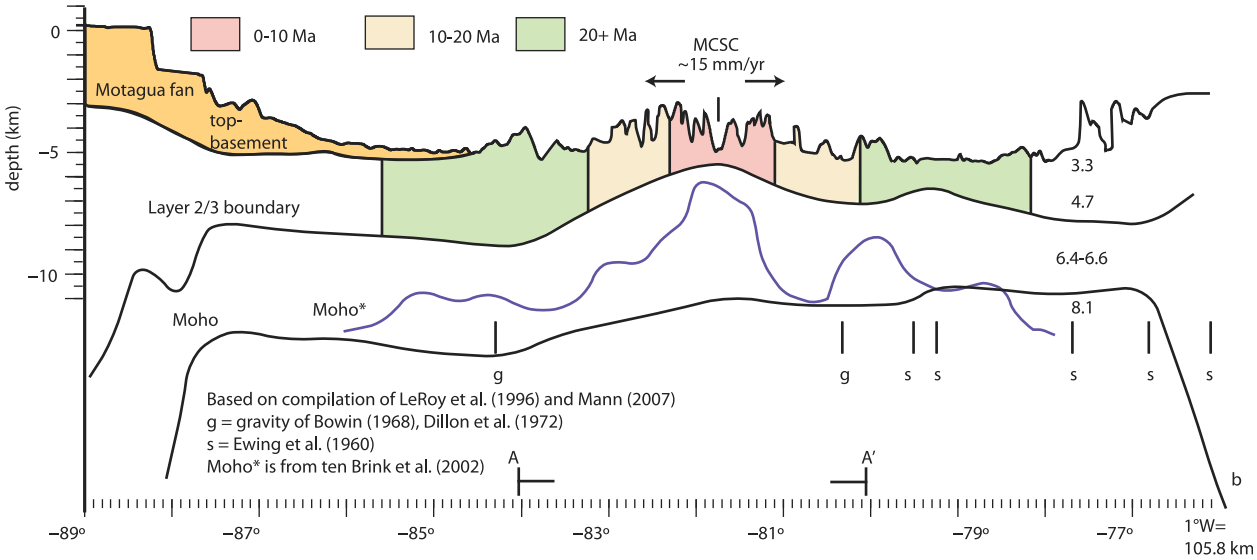

Figure 2. Cross section across the Cayman trough after *Mann* [2007] and *Leroy et al.* [2000] with alternative interpretations of seismic velocity and gravity data for the surface of the Moho. A-A′ location is shown on Figure 1. Labeled tick marks "s" and "g" are from along-strike surveys (i.e., into the plane of the page) [*Dillon et al.*, 1972].

1970s human occupied vehicle Alvin dive tracks, along with summary pie charts illustrating the relative proportion of basalt, gabbro, and peridotite samples from each dive. We also overlay dredge locations colored by major lithology on the map (also see Figure 1). As explained below, the major lithologic categories are simplifications of a petrologically richer sample suite (Tables S1 to S3).[1] Although many of the samples dredged in the 1970s are no longer available for study, they all were systematically documented, and some studied in great detail [*Perfit*, 1977; *Perfit and Heezen*, 1978]. To support our summary and interpretations of the three CAYVIC ROV Victor dives, we provide sample descriptions and dive maps in Table S3 and Figures S1 to S3, but leave detailed petrologic and structural studies for a separate effort.

[12] The bathymetric structure of the MCSC is defined by ~5 to >6 km deep basins within an axial rift bound by domal massifs and more planar rift walls that approach ~2 km below sea level. Young volcanic features characterize the relatively shallow centers of the central intrarift ridges. The southern intrarift ridge trends obliquely to the rift walls and may be more fault-controlled, whereas the northern intrarift ridge trends roughly parallel to the rift walls. Locally, volcanic edifices mark the volcanic fields, particularly in the northern area of the rift (see arrow within inset of Figure 3).

[13] The southern ridge trends NNW directly into the west central massif called "Mount Dent" by *Edgar et al.* [1991]. Mount Dent is one of three massifs with curviplanar surfaces that dip shallowly toward the center of the rift; the other two are at the northeast ridge-transform intersection and the southeastern area of the rift wall. The relatively smooth surface of Mount Dent is cut by a series of NS striking scarps identified by *Stroup and Fox* [1981]. A series of EW scarps also cut the massif, the most prominent along the southern face of the massif that was interpreted to be a nontransform offset by *Macdonald and Holcombe* [1978]. Otherwise, the eastern flank of Mount Dent extends along its gently sloping surface into the central area of the rift where it intersects the north central intrarift ridge, and defines the northern boundary of the deep central basin. In contrast, the west flank of Mount Dent is a relatively linear (in map view) rift wall.

[14] Through our compilation of major rock types, the geology of the MCSC comes further into focus. The deeper basins and linear ridges within the rift are dominated by basaltic lavas, although peridotite and gabbro have been dredged from both the northern and southern parts of the central rift. There are few constraints on the geology of the steeper walled rift flanks, but dredging and deep-sea vehicle sampling from the flanks of the shallowly dipping massif recovered a mix of gabbro and peridotite, and at least one of the rift walls (to the southeast) appears to comprise mostly basalt. In

[1] Auxiliary materials are available in the HTML. doi:10.1029/2010GC003240.

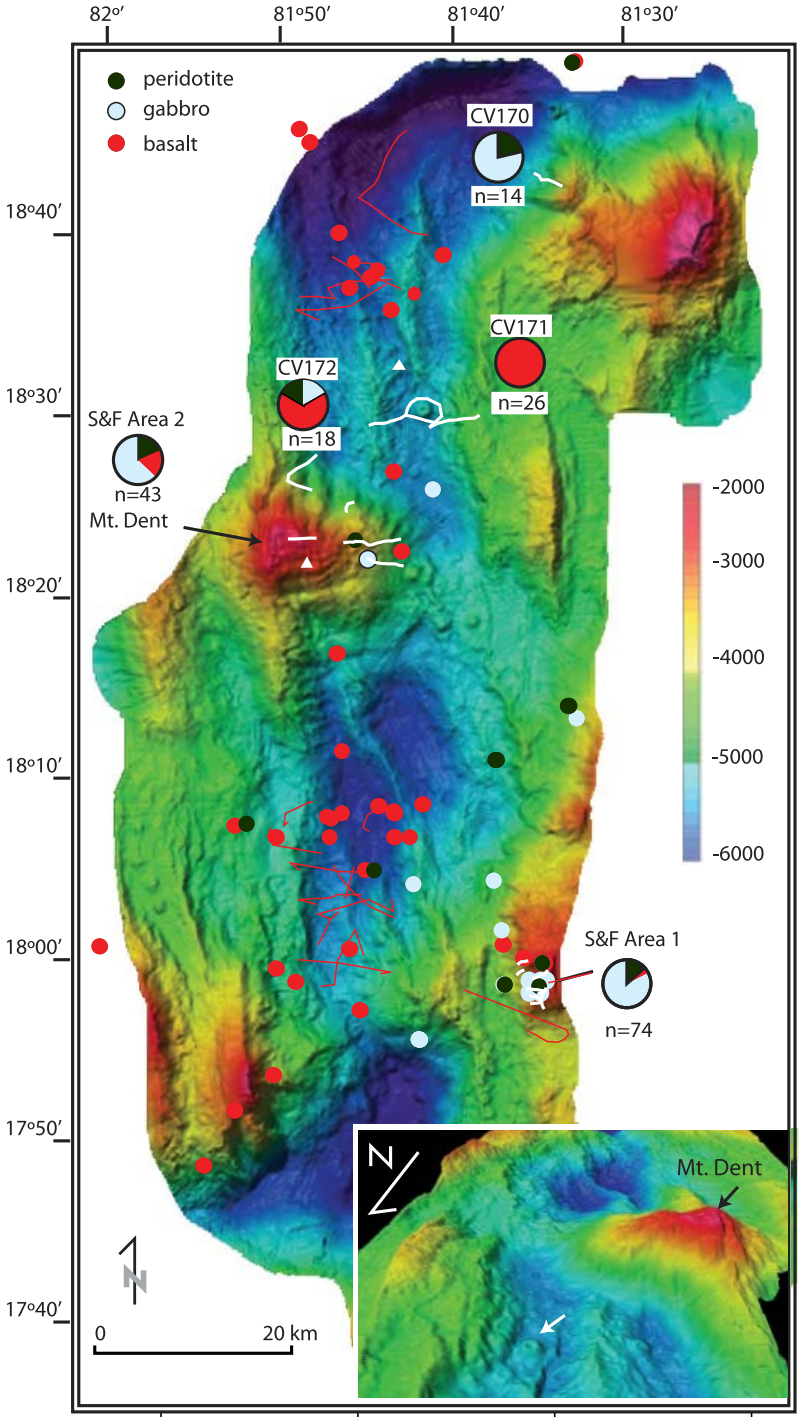

Figure 3. Multibeam bathymetry of the Mid-Cayman Spreading Center collected during the 2002 CAYVIC cruise. Colored dots indicate dredged samples (see key). White lines are the Alvin dive areas of *CAYTROUGH* [1979] as described in full by *Stroup and Fox* [1981] ("S&F") and the CAYVIC (CV) ROV Victor 6000 dives. Pie charts indicate the relative abundance of different lithologies for each dive area (see Tables S1–S3 and text for more detailed descriptions). Red lines are the "Angus" tow tracks, a deeply towed camera used during the *CAYTROUGH* [1979] project. Small white triangles on Mount Dent and the northern volcanic field are the approximate locations of active hydrothermal vents. The inset is a south facing, oblique view of the volcanic ridge adjacent to high-angle scarps in the foreground, and the more gently dipping surface of Mount Dent.

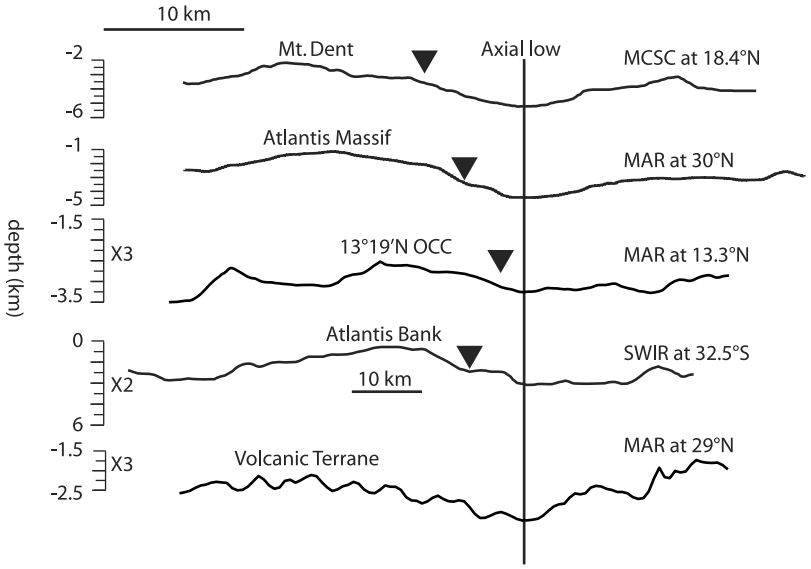

Figure 4. Cross-axis bathymetric profiles across with triangles marking the approximate position of the "termination" or map trace of the inferred detachment fault: (top to bottom) Mount Dent and the MCSC from the bathymetry presented in Figure 3, the Atlantis Massif at MAR 30°N from http://www.geomapapp.org; the 13°19′N MAR OCC from *Smith et al.* [2008] (note vertical exaggeration), the ~14 Ma Atlantis Bank south of the SWIR from *Muller et al.* [2000] (note vertical exaggeration and difference in horizontal scale from other profiles), and across the volcanic segment of the MAR at 29°N from http://www.geomapapp.org (note vertical exaggeration).

contrast, the massifs such as Mount Dent appear to be dominated by gabbroic rocks and peridotite, and some basalt; off-axis basaltic samples have not been carefully studied to date but could include lavas (tectonically transported and/or erupted off axis), and likely include variably altered intrusive units (Tables S1 to S3).

[15] Many of the bathymetric features of the MCSC resemble those observed on other slow-and ultraslow spread MORs such as the MAR or the SWIR. For example, Mount Dent has a curviplanar surface similar to that observed on the Atlantis Massif on the MAR at 30°N [e.g., *Cann et al.*, 1997] and the Atlantis Bank off the SWIR axis [e.g., *Miranda and John*, 2010], and is flanked to the west by linear ridges similar to those observed at 13°19′N on the MAR [*Smith et al.*, 2006, 2008; *MacLeod et al.*, 2009]. The apparent similarities between these massifs are reinforced in two-dimensional profiles across these different features (Figure 4). Both Mount Dent and the Atlantis Massif share a crest to trough wavelength of 15–20 km and an axial low to massif summit amplitude of ~4 km. Intriguingly, neither the 13°19′N massif, nor the Atlantis Bank share the same amplitude and/or wavelength with Mount Dent or the Atlantis Massif, though the overall structures are similar. In contrast, segments of the MAR with abundant volcanics and seafloor fabrics have much different cross-axis profiles typified by abyssal hills and steeply dipping faults, as illustrated by 29°N [e.g., *Escartín et al.*, 1999]. A similar comparison between the MCSC and ultraslow spreading centers such as the Gakkel, Knippovich, and other segments of the SWIR would be very informative, but is not straightforward given the paucity of geologic data for such ridges, and their diverse axial morphologies [*Cochran et al.*, 2003; *Cannat et al.*, 2006, 2008].

4. Aeromagnetic Data From the MCSC and Cayman Trough

[16] In order to better understand the nature of Cayman trough crust, we describe its magnetic structure in the context of the aforementioned bathymetric and geologic structure. Ultimately, a better understanding of the Cayman trough crust will also require new data acquisition to build on the shipboard and satellite gravity data analysis of *ten Brink et al.* [2002], as well early seismic [*Ewing et al.*, 1960], gravity [*Bowin*, 1968], and heat flow [*Erickson et al.*, 1972] studies. The focus on the aeromagnetic data here is (1) to clarify the spreading history of the MCSC, which to date has been resolved through seafloor magnetic anomaly data collected by the 1973 R/V *Wilkes* cruise [*Rosencrantz et al.*, 1988; *Leroy et al.*, 2000] and

(2) to use magnetic data to evaluate the distribution of basaltic lava, gabbro, and peridotite.

[17] Aeromagnetic data were collected by a 1992 BGM Airborne Surveys Inc. survey of the central Cayman trough (Figure 5a) [*Rosencrantz*, 1995]. The aeromagnetic data were collected with a resolution of 0.001 nanoTesla (nT), a cycle rate of 0.2 s, and sample interval of 17 m, and corrected for the 1990 International Geomagnetic Reference Frame (IGRF). The survey was flown at a height of 305 m above the sea surface with a line spacing of ~6 km. A diurnal correction was applied (with a base value of 41800 nT) and the data were downward continued to sea level. Additional corrections to "detrend" the data were applied to correct for a strong gradient in magnetic intensity from south to north across the trough and the low latitude of the location.

[18] In order to evaluate magnetizations as well as magnetic anomalies, an inversion of the magnetic anomaly data was performed using the two-dimensional method of *Parker and Huestis* [1974], extended to three dimensions by *Macdonald et al.* [1980]. A 1 km thick magnetic source layer, bounded on top by a composite bathymetry grid extracted from the Global MultiResolution Topography (GMRT) data set and resampled to a 1 km grid spacing. A cosine taper bandpass filter with a low-cut taper from 150 to 300 km and a high-cut taper from 4 to 8 km assured convergence of the inversion. The topography was mirrored at the edges to minimize edge effects caused by the assumed periodicity of the FFT calculations in the inversion. A crustal magnetization parallel to a geocentric axial dipole was assumed. The magnetization data were gridded at a resolution of 1 km to match the resolution limit of the bathymetry grid. A magnetic annihilator was not applied to the result of the inversion.

[19] The most significant result from our analysis is that the magnetic field *and* the magnetizations are heterogeneous across the MCSC (Figures 5a and 5b). Similar to areas along the MAR [*Fujiwara and Fujimoto*, 1998; *Smith et al.*, 2008] and the SWIR [*Sauter et al.*, 2008], the magnetic anomaly data over the Cayman trough is quite "patchy," with magnetic highs and lows that crudely correlate with bathymetric highs and lows. Though *Sauter et al.* [2008] and *Fujiwara and Fujimoto* [1998] (among others) have noted that even nonvolcanic crust produces magnetic anomalies, most such analyses find that volcanic crust has higher magnetization than nonvolcanic crust. Therefore, given the distribution of rock types in the MCSC and surrounding Cayman trough (Figures 1 and 3), the interpretation of the aeromagnetic anomaly and magnetization pattern is relatively straightforward: Mount Dent and the other massifs comprising predominantly gabbro and peridotite display relatively low magnetizations and somewhat depressed magnetic anomalies, whereas the basaltic volcanic fields display high magnetizations and enhanced magnetic anomalies.

[20] If our correlation of high magnetization and basaltic lavas is correct, then it further suggests that MCSC seafloor spreading has episodically produced such massifs (i.e., OCCs) since at least early Miocene time, if not before. The reason for this interpretation is the pattern of reversals in the magnetization model (Figure 5c). Namely, to the east of the MCSC, one can clearly delineate striped magnetic reversals in the magnetization model at least back to anomaly 6 (~20 Ma). The stripes are not uniform, however, but widen and narrow along their map trace. The shape of the reversals is therefore consistent with irregularly shaped basaltic basins along the paleoridge axis. In contrast, the magnetization pattern to the west of the MCSC is extraordinarily irregular, to the point that reversals cannot be clearly identified. We therefore suggest that the seafloor to the west of the MCSC is dominated by gabbro and peridotite, and some scattered lavas, whereas to the east the seafloor is dominated by basaltic lavas that record the magnetic reversals more clearly.

[21] The aeromagnetic data and magnetization model also explain some of the historic difficulty in the interpretation of the spreading history. *Rosencrantz et al.* [1988] determined that spreading rates were ~15 mm/yr since 25–30 Ma, before which they were considerably faster (20–30 mm/yr). In contrast, *Leroy et al.* [2000] determined that spreading rates were ~17 mm/yr for the last ~20 Ma, prior to which they were ~15 mm/yr, but with a very early faster (~20 mm/yr) spreading rate. The difference between the two solutions undoubtedly arose because of the general poor definition of the anomalies in shipboard data, particularly to the west of the MCSC. Additionally, the anomalies vary in their widths and positions across the trough, partly due to a combination of nontransform offsets [*Macdonald and Holcombe*, 1978] and ridge propagation [*Leroy et al.*, 2000].

[22] By superposing the magnetic anomaly model of *Leroy et al.* [2000] on our magnetization model (Figure 5c) (the model of *Rosencrantz et al.* [1988]

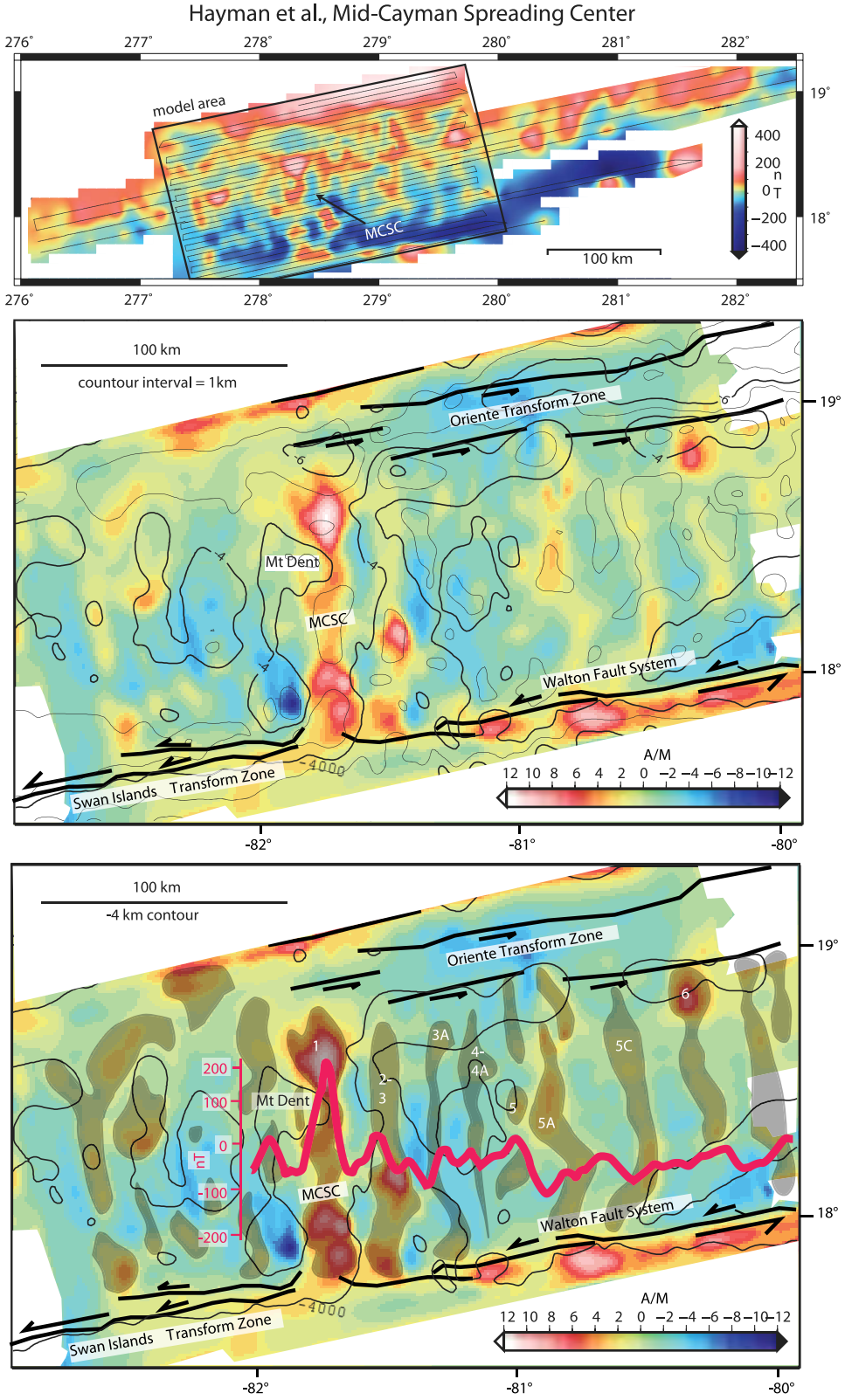
Hayman et al., Mid-Cayman Spreading Center
276°
277°
278°
279°
280°
281°
282°
19°
18°
model area
MCSC
100 km
400
200
nT
0
−200
−400
100 km
countour interval = 1km
Oriente Transform Zone
Mt Dent
MCSC
Walton Fault System
Swan Islands Transform Zone
A/M
12 10 8 6 4 2 0 −2 −4 −6 −8 −10 −12
-82°
-81°
-80°
100 km
-4 km contour
200
100
0
-100
-200
nT
1
2-3
3A
4-4A
5
5A
5C
6

Figure 5

did not correlate well with these newer aeromagnetic data), we were able to clearly delineate several of the magnetic reversals such as the Brunhes/Matuyama (~0.8 Ma) and younger boundary of anomaly 2 (~1.6 Ma). However, because of the ultraslow spreading rate, many of the reversals are indistinguishable; for example, anomalies 2 and 3 (~5.7 Ma) are indistinguishable from one another to the east of the MCSC. According to our interpretation, anomaly 6 (~20 Ma) is the prominent area of high positive magnetization near the eastern edge of the magnetization model (see Figure 5b), which yields a full spreading rate of ~15 mm/yr. The same exercise for different anomalies at different positions in the trough produces spreading rate solutions from 15 to 17 mm/yr.

[23] There is also some controversy about the older parts of the Cayman trough. As mentioned previously, *Leroy et al.* [2000] argued that the magnetic anomaly record extended back to ~49 Ma (anomaly 22). In contrast, *ten Brink et al.* [2002] argued that much of the older Cayman trough crust is transitional between oceanic and continental, and not the product of seafloor spreading (though perhaps a nonvolcanic spreading history would still be consistent with *ten Brink et al.*'s [2002] model). The aeromagnetic data do not completely solve this problem of the nature of older Cayman trough crust, but do find that there are areas of positive and negative polarity in the magnetic anomaly data (Figure 5a, eastern edge outside of the magnetization model area). We therefore accept the findings of *Leroy et al.* [2000] barring further data acquisition in the region.

5. Microstructure, Petrology, and Geochemistry of Rocks Sampled From the MCSC

[24] Having described the lithologic and magnetic map patterns of the Cayman trough, we now turn our attention to the nature of the geological samples collected from the MCSC. We note that sampling of the MCSC to date has not been of very high resolution in the sense that dredged samples were obtained prior to modern shipboard navigation and are not groundtruthed to seafloor structures. Furthermore, samples from near-bottom investigations can only be qualitatively positioned relative to an inferred, but largely unmapped, detachment fault. Nonetheless, there are sufficient samples from the 1970s dredge and dive programs to establish some of the microstrucural, petrological, and geochemical characteristics of these rocks, which provide further constraints on the crystallization, deformational, and metamorphic history of the MCSC. Some of the available data stems from previously published work, although we focus here on previously unpublished petrographic (optical microscopy) observations and geochemical analyses from *Perez-Suarez* [2001]. Again, we leave detailed analyses of the 2002 CAYVIC samples (Table S3 and Figures S1 to S3) to a future, separate effort.

[25] The rocks sampled from the MCSC are actually quite diverse and in many samples exhibit mixed lithologies and contact relationships even on hand sample scales. Rock types include: peridotite (harzburgite and lherzolite), dunite, trOctolite, olivine gabbro, gabbro, gabbronorite, anorthositic gabbro, trondjhemite, and ferrogabbro (Tables S1 to S3). In general, peridotites are pervasively altered to serpentinite, but the mesh texture and relict mineral grains allow for the identification of protoliths: lherzolites contain olivine (to $Fo_{91.0}$), orthopyroxene (Mg# $\leq$ 90.2) and clinopyroxene (Mg# $\leq$ 91.2). Many of the dredged samples are only slightly altered with up to centimeter-scale primary igneous crystals. Alteration phases in the troctolites are localized to grain boundaries, allowing identification of the original poikilitic granoblastic texture of olivine crystals embedded in and surrounded by subhedral plagioclase crystals (with abundant growth twinning) and pyroxene grains. Troctolites are commonly quite plagioclase rich. Olivine gabbros (>5% olivine), gabbronorites (with abundant orthopyroxene), and gabbros have poikilitic (plagioclase and pyroxene surrounding olivine) and ophitic (pyroxene-plagioclase) textures. In the few samples where contacts are pre-

Figure 5. (a) Magnetic anomaly map of the Cayman trough from aeromagnetic data collected in 1991. Thin lines are flight lines and MCSC is in the center of the Mid-Cayman Spreading Center. (b) Magnetization model of the boxed area of Figure 5a. Mount Dent and other key structural features are indicated, along with the −2, −4, and −6 km bathymetric contour. See text for more details. (c) The magnetization model with areas of normal polarity shaded (by inspection). Superposed on the map is the magnetic anomaly profile modeled by *Leroy et al.* [2000] based on the 1973 R/V *Wilkes* profiles and our interpreted normal polarity intervals. Key ages are (again, from *Leroy et al.* [2000]) 0.78 Ma for the edge of anomaly 1, 5.96 Ma for the youngest edge of anomaly 3A, 10.24 for the oldest edge of anomaly 5, and 20.26 Ma for the oldest edge of anomaly 6; ages will differ depending on the magnetic time scale used.

served, anorthositic gabbros and ferrogabbros intrude their host rock. Last, diabasic intrusions have been identified and basalts range from glassy and fresh to hydrothermally altered, though we cannot at present delineate spatial-temporal histories of basalt/diabase intrusions and their hydrothermal histories.

[26] Many of the rocks from the massif were deformed at amphibolites to granulite facies conditions (~650°C–850°C) as indicated by dynamically recrystallized brown amphibole, pyroxene, and plagioclase laths that define metamorphic foliations, and kinked twins in plagioclase grains (Figure 6) [*Malcolm*, 1981; *Ito and Anderson*, 1983; *Karson and Fox*, 1986]. A sense of the quantity and distribution of the deformed gabbros comes from the maps of *Stroup and Fox* [1981] who described metagabbros, gneisses, and amphibolites at ~8 locations on the east flank of Mount Dent between 3.6 and 2.8 km depth, and ~3 locations on the southeastern massif. CAYVIC dive 170 on the northeastern massif traversed foliated gabbros, whereas CAYVIC dive 172 on the north side of Mount Dent traversed mixed basalt and peridotite breccias (Tables S1 to S3 and Figures S1 to S3). At least five dredge hauls taken over the years yielded gabbroic samples with kinked or dynamically recrystallized crystals. Given the observations available, it appears that deformed gabbros comprise a major part of the curviplanar surfaces of Mount Dent and the other two MCSC massifs.

[27] Greenschist minerals in the gabbros are dominated by vein- and vug-filling brown and green amphibole, serpentine, chlorite, and other phyllosilicates. These veins and vugs crosscut the foliations and mylonitic shear zones, and alteration minerals are also common in cataclastic microstructures [*Malcolm*, 1981]. *Ito and Clayton* [1983] ascribed oxygen isotope compositions of secondary phases to greenschist to amphibolite facies conditions of metamorphism with seawater infiltration at <~700°C. Future work is required for more exact interpretations of the microstructural properties of the MCSC samples in the context of inferred detachments, as has been successfully accomplished through more comprehensive near-bottom investigations elsewhere [e.g., *Schroeder and John*, 2004; *Harigane et al.*, 2008; *Miranda and John*, 2010].

[28] The mineralogy and crystallization history of the MCSC basalts and gabbros also allows us to place the MCSC in a global context of spreading-center processes. The primary igneous mineralogy and geochemistry of these rocks are here first viewed as a direct result of mantle conditions, largely because of clinopyroxene compositions and phase relations [e.g., *Herzberg*, 2004]. Later, we consider the potential role of crustal mush zone and OCC development in the petrogenesis of basalts and gabbros. MCSC basalts are moderately evolved and relatively homogenous as a group (Figure 7). The major element compositions of MCSC basalts have been cited as type examples of MORBs extracted via low extents of melting from a relatively homogenous "cold" mantle [*Klein and Langmuir*, 1987, *Elthon et al.*, 1995]. Importantly, they have unusually high $Na_{8.0}$ values (3.16–3.25) and low $Fe_{8.0}$ values (7.1–7.23) (Na_2O and FeO concentrations normalized to 8 wt. % MgO) compared to most other MORB, suggested by *Klein and Langmuir* [1987] to represent an end-member composition of global MORB compositions. Additionally, CaO-Al_2O_3-MgO variations in MCSC basalts led to suggestions that evolving MCSC melts were multiply saturated with olivine + plagioclase + pyroxene, requiring pressures of crystallization as high as 5–6 kbar [*Elthon et al.*, 1995], consistent with data from phases in MCSC gabbros [*Elthon*, 1987, *Perez-Suarez*, 2001]. Similar petrogenetic scenarios have been discussed in other MOR settings [e.g., *Eason and Sinton*, 2006].

[29] Major element variations in Cayman gabbroic rocks are similar to, but less extreme in their compositional range than those in comparable settings, such as the Atlantis massif at 30°N on the MAR [*Godard et al.*, 2009] (i.e., consider MgO variations in Figure 7). In addition, they display a much greater compositional variation than MCSC glasses [*Thompson et al.*, 1980] and spatially related basalts and diabases (Figure 7). Trends in the lava and glass major element data reflect the evolution of primitive liquids via crystal fractionation (of olivine + plagioclase + pyroxene) whereas the spread in gabbro data result from the accumulation of near-liquidus phases in variable proportions as well as the addition of intercumulus melts. For example, elemental trends toward high-Al_2O_3 and low-FeO contents reflect the accumulation of plagioclase in many of the troctolites, gabbros and anorthositic gabbros whereas more mafic samples show the effects of olivine and pyroxene accumulation (Figure 7). *Elthon et al.* [1995] suggested the major and trace element variations in MCSC basalt glasses are consistent with the extraction of olivine gabbro cumulates from a range of potential primary magmas.

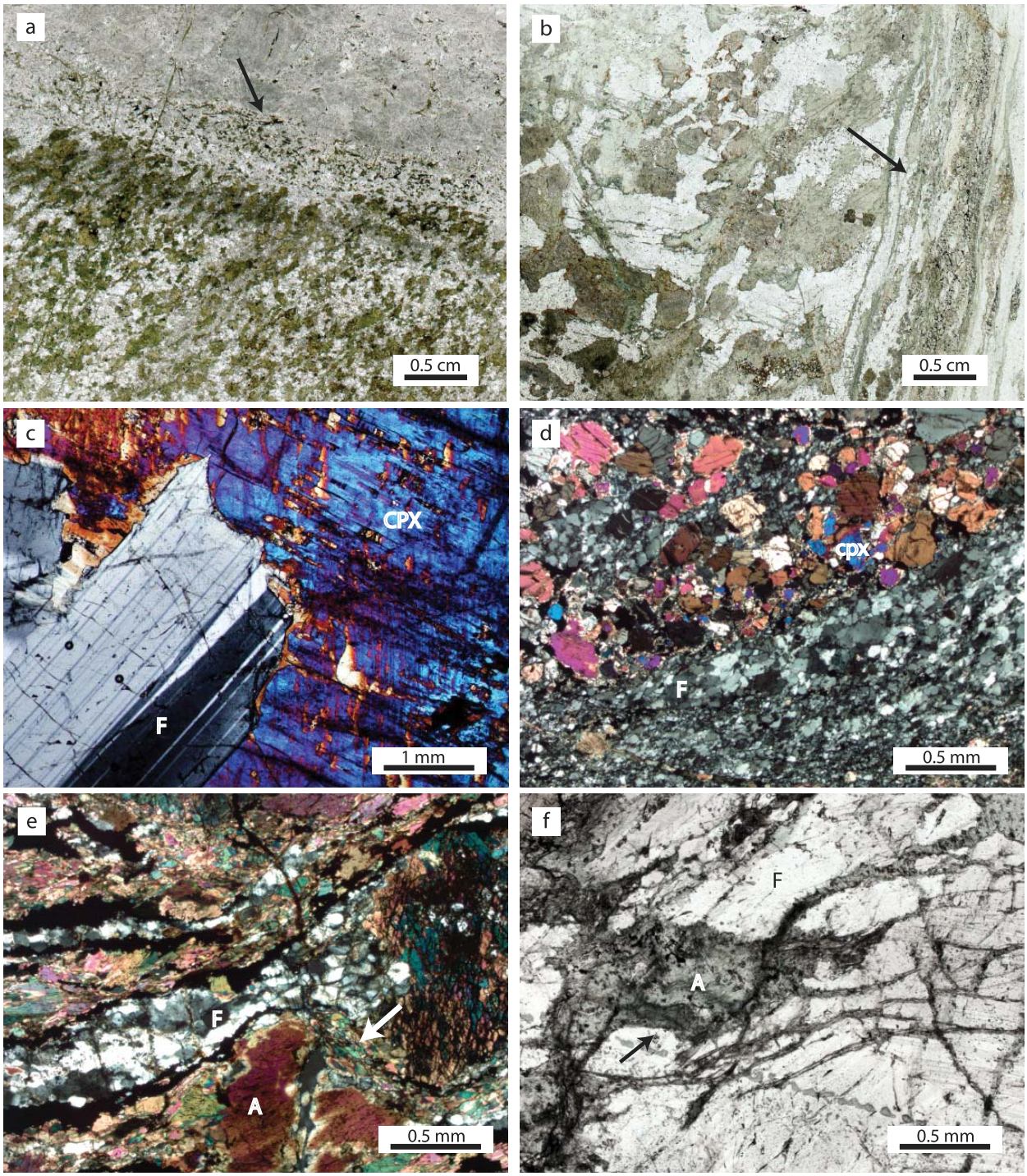

Figure 6. Microstructure of MCSC gabbros. (a) Sample E702-H: intrusive contact between trondhjemite and gabbro (indicated by arrow). Amphibole and some relict pyroxene grains make up the mafic (greenish) phases, and feldspar (anorthite, minor albite) comprise the felsic (clear to gray) phases. (b) Alv-612-3-1: mylonitic shear zone (indicated by arrow) crosscuts variably altered coarse-grained gabbro. (c) Alv-615-1-1: coarse-grained, relatively unaltered gabbro with poikoilitic clinopyroxene (cpx) and feldspar (F) laths. (d) Alv-612-3-1: mylonitic shear zone with dynamically recrystallized plagioclase (F) and pyroxene (cpx) grains. (e) Alv 616-7-1: mylonite with stretched aggregates of magnetite-ilmenite (opaque), plagioclase (F), and hornblende (A), including dynamic recrystallization of amphibole (marked by white arrow). (f) Alv-738-1-1: microcracks filled with chlorite and actinolite (A) (likely replacing pyroxene) crosscut feldspar-rich (F) gabbro.

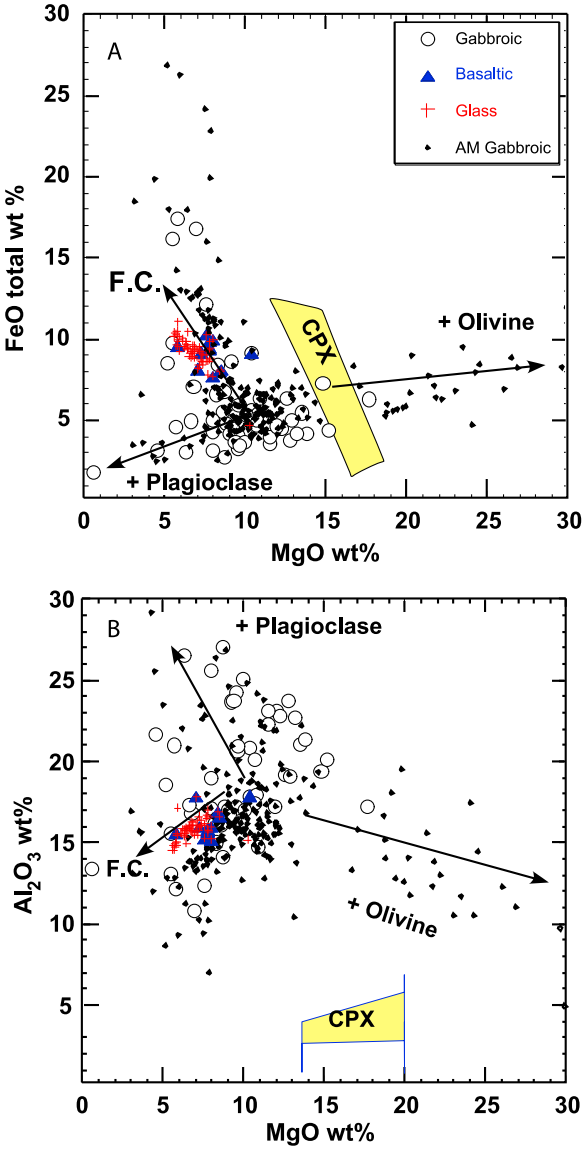

Figure 7. Major element diagrams showing variations in (a) FeO (total) wt% versus MgO wt% and (b) Al_2O_3 wt% versus MgO wt% in gabbroic rocks (open circles), basaltic rocks (solid triangles), including diabase as compared to gabbroic rocks from the IODP Hole 1309D (small trapezoids) on the Atlantis Massif, Mid Atlantic Ridge at ~30°N [*Godard et al.*, 2009], and basaltic glasses from the Mid-Cayman Spreading Center [*Thompson et al.*, 1980; *Elthon et al.*, 1995]. Arrows point in the general directions expected from fractional crystallization (FC) of plagioclase, olivine, and clinopyroxene, plagioclase accumulation, and olivine accumulation. The compositional field of clinopyroxenes in the MCSC gabbros discussed here is also shown. Note the similarities of Cayman gabbroic rocks to those recovered from the Atlantis Massif and the very limited range of basalt compositions.

[30] The relatively homogeneous compositions of MCSC basalts (Figures 7 and 8) may be a consequence of efficient magma mixing in subaxial magma lenses and mush zone, or it may simply reflect the limited spatial sampling that has been done to date. Nonetheless, volcanic and plutonic rocks recovered from the MCSC exhibit a large range of chondrite-normalized rare earth element (REE) patterns, from very light REE depleted peridotites to slightly light REE enriched basalts and ferrogabbros (Figure 8). Some cumulate gabbros have low incompatible element and REE abundances and commonly have characteristic positive Eu anomalies indicative of plagioclase accumulation. More evolved gabbros have REE patterns similar to Cayman basalts and diabases. The most evolved ferrogabbros exhibit elevated REE contents and negative Eu anomalies indicative of plagioclase fractionation and consistent with their relatively low Al_2O_3 contents. The range of REE patterns is typical of plutonic rocks from slow spread ridges and established OCC settings elsewhere [e.g., *Dick et al.*, 2000; *Coogan et al.*, 2000; *Godard et al.*, 2009].

[31] Overall, the REE patterns and REE contents in clinopyroxenes in gabbros and peridotites [*Perez-Suarez*, 2001] suggest that a diversity of parental melts were involved in the petrogenesis of MCSC rocks. *Elthon et al.* [1995] also noted that incompatible element compositions varied widely between samples suggesting a variety of parental melts and or reactions with gabbroic rocks within the lower crust.

6. Discussion

[32] The structure and spreading history of the MCSC are of global significance for several reasons. The MCSC may provide an active example of OCC development as key to ultraslow spreading-center processes, as proposed for segments of SWIR spread crust [e.g., *Cannat et al.*, 2006]. The MCSC could also extend the linkage between hydrothermal processes and OCCs [e.g., *McCaig et al.*, 2007] to ultraslow spreading rates. The asymmetric bathymetry and magnetic structure of the Cayman trough, the distribution of different lithologies, and the spreading-center history, all within a very narrow and geographically accessible strip of oceanic crust, combine to make the Cayman trough an excellent testing ground for controls on OCC development and ultraslow spreading processes. Last, because the MCSC has long been cited as an end-member in the spreading-center

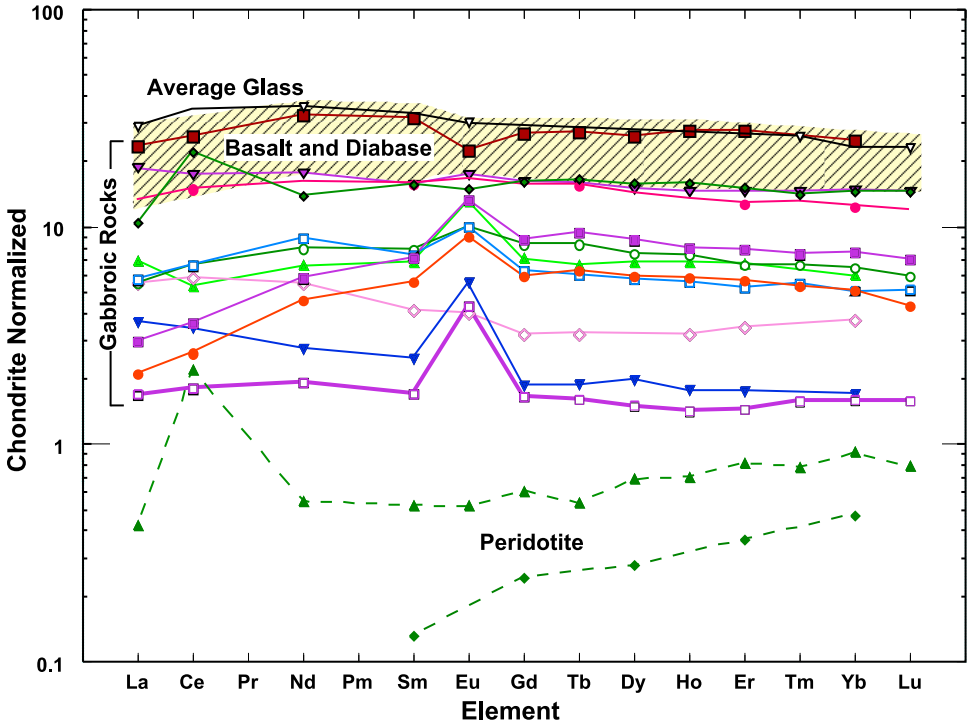

Figure 8. Chondrite-normalized [*Sun and McDonough*, 1989] rare earth element diagram showing the range of REE abundances and patterns in rocks ranging from peridotite to basalt from the Mid-Cayman Spreading Center. Peridotites have very low abundances and significant depletions in light REE (the positive Ce- anomaly is a consequence of seawater alteration associated with serpentinization). Gabbroic rocks have a wide range of compositions with plagioclase-rich samples having low REE abundances and positive Eu anomalies. More evolved gabbronorites and ferrogabbros have elevated REE abundances and some have negative Eu anomalies reflecting their more evolved nature and the effects of plagioclase fractionation. Pattterns such as these are very typical of peridotites and gabbroic rocks from oceanic core complexes [e.g., *Godard et al.*, 2009]. Shaded field represents the range of REE in basaltic rocks and the "average glass" composition [from *Thompson et al.*, 1980] and is the uppermost pattern plotted. Both LREE depleted and enriched samples are present in the suite of rocks recovered.

spectrum [e.g., *Klein and Langmuir*, 1987], it is logical to establish the controls on ultraslow crustal structure at the MCSC.

[33] A highly interpretive geological map of the MCSC provides a context for MCSC crustal accretion (Figure 9). The map is generally faithful to the currently known distribution of rock types, structures, and major bathymetric features, and depicts curviplanar detachment faults that separate the volcanics from the underlying basement lithologies (gabbroic rocks and peridotites, with some intrusive basalts). Within the intraridge rift, the northern and southern basaltic volcanic fields dominate the seafloor. High-angle faults cut across both the massifs and basaltic volcanic fields, including the detachment faults in places. Last, hydrothermal vents have been located within the northern volcanic field, and also off axis on Mount Dent. The axial vent is a black smoker system, whereas the off-axis vent produces vigorous, moderate-temperature discharge of clear fluids, producing a sulfide and sulphate chimney [*Murton et al.*, 2010], but with a complicated plume signal perhaps owing to a contribution from fluid-ultramafic rock reactions [*German et al.*, 2010].

[34] We thus develop a general genetic model for the evolution of the map pattern described above, beginning with the melt history leading to accretion of the gabbroic crust (Figure 10). Though melt supply to the MCSC may have been from a deeper mantle source, we envision that the MCSC gabbros crystallized within a lower pressure mush zone(s) subjected to multiple intrusions of basaltic to ferrobasaltic residual melts. This magmatic scenario is similar to that proposed for ridges where gabbroic and ultramafic rocks are exposed at OCC such as in the SWIR and MAR, and also suggested to be an important control on MORB composition [*Lissenberg and Dick*, 2008; *Dick et al.*, 2010; *Escartín et al.*, 2008; *Suhr et al.*, 2008a, 2008b; *Godard et al.*,

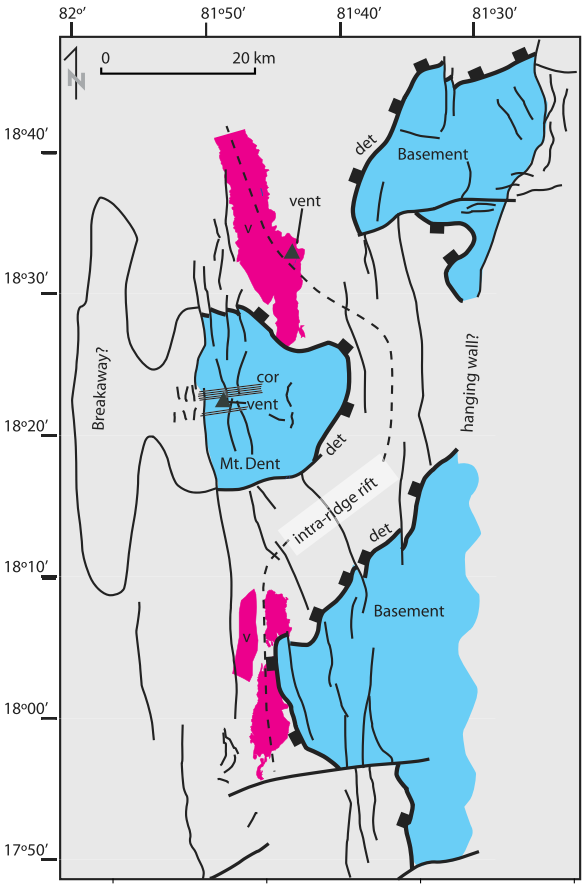

Figure 9. Highly interpretive geologic map of the MCSC based on bathymetry and dive and dredge compilation. Thick barbed lines are detachments bounding basement rocks (gabbro, peridotite, intrusive basalts) shaded in blue. Steeply dipping faults are thin, undecorated lines. Basaltic volcanic fields are in red, and triangles mark hydrothermal vent localities.

2009]. The mush zone model for the MCSC explains the discrepancy between a proposed relatively uniform mantle source and the diverse compositions and mineralogy of the gabbros [*Elthon*, 1987; *Elthon et al.*, 1995]. These intrusions left behind various proportions of cumulate crystals resulting in olivine-rich and anorthositic gabbros, intercollated with peridotites, and undoubtedly more pyroxene-rich rocks as well.

[35] It is worth noting that recent results from other ultraslow spreading centers point to rich relationships between crustal magmatic processes, such as we envision for the MCSC, and upper mantle heterogeneity. Recent geochemical studies of MORB erupted along slow and ultraslow spreading centers [*Cannat et al.*, 2008; *Escartín et al.*, 2008; *Standish et al.*, 2008] have pointed to the complex controls on melt chemistry, and noted that mantle heterogeneity can affect melt composition *and* spreading geometry, which can in turn affect thermal structure and thus extents of melting. Other petrologic and geochemical studies of slow and ultraslow spread crust further suggest that many of the unique compositional properties may result from melt transport coupled with deformational processes, rather than as a simple function of mantle temperature [e.g., *Natland and Dick*, 2001; *Gao et al.*, 2007; *Dick et al.*, 2010].

[36] Following assembly of the lower crustal and upper mantle rocks that comprise the massifs (blue in Figure 9), deformational processes accommodated their exhumation. Such deformational processes nearly (and may locally) overlap in space and time with melt conditions in many settings, as inferred from interpreted melt-shear zone relationships in places like the SWIR [*Dick et al.*, 2000], and granulite facies shear zones in places such as the Atlantis Massif [*Blackman et al.*, 2006]. Such a deformational history applies to the MCSC rocks as well, though high-strain zones also developed at somewhat lower, amphibolite facies temperatures associated with syntectonic hydrothermal fluid flow at <~700°C [*Ito and Anderson*, 1983; *Ito and Clayton*, 1983]; temperatures of amphibolite facies deformation in OCCs worldwide have been suggested by others to range from 550°C–850°C [*Schroeder and John*, 2004; *Harigane et al.*, 2008; *Michibayashi et al.*, 2008; *Miranda and John*, 2010]. Similar to the Atlantis Massif and other OCC settings, high-temperature shear in the MCSC gave way to "static" filling of veins, vugs, and grain boundary interstices by greenschist facies minerals. The fluids responsible for this greenschist facies alteration likely fed seafloor hydrothermal vents [e.g., *McCaig et al.*, 2007]. Greenschist facies minerals are also found in cataclasites, suggesting that hydrothermal alteration overlapped with late stages of exhumation [*Stroup and Fox*, 1981; *Ito and Anderson*, 1983].

[37] We further suggest that the OCC model likely applies to accretion of older Cayman trough crust (Figure 10). This hypothesis is supported by a few off-axis dredges (Figure 1) and patterns in the aeromagnetic data and magnetization model (Figure 5) that suggest that the same distribution of rock types across bathymetric highs and lows in the axial MCSC may also be present in the off-axis regions in the Cayman trough. Additionally, the bathymetry of the off-axis Cayman trough is highly asymmetric with relatively shallow, mountainous bathymetry to the west, and deep basins on the

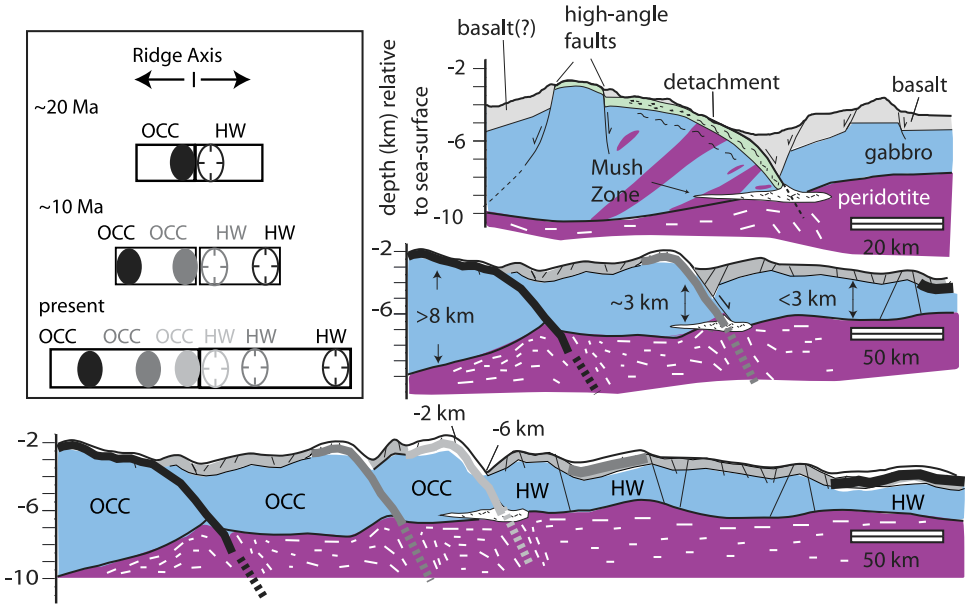

Figure 10. (inset) Schematic map view of Cayman trough seafloor spreading since ~20 Ma. Each ellipse is the map trace of an ancient and/or active OCC at different geological times, with the basaltic hanging walls systematically stripped off to the east and the footwalls spread to the west. Cross-sectional views drawn on bathymetric profiles across 18.4°N (Mount Dent) of each stage are presented with (top) cross-sectional view showing hypothetical distributions of peridotite (purple)-gabbro (blue)-basalt (gray) intrusive and structural relationships, including hypothesized greenschist-grade (e.g., serpentinite) detachment shear zone (green). (middle and bottom) Generalization of the crustal section in order to illustrate the crustal thickness and bathymetric variations that can arise via ongoing OCC development.

conjugate crust to the east (Figure 1). Such asymmetry is also observed in sparse heat flow data [*Erickson et al.*, 1972; *Rosencrantz et al.*, 1988]. The crustal thickness, though poorly constrained, is thought to be highly asymmetric as well, with thinner upper crust to the east than west, and an irregular estimated Moho depth [*Leroy et al.*, 2000; *ten Brink et al.*, 2002] (Figure 2).

[38] The OCC model potentially accounts for the inferred crustal thickness variations through the exhumation of lower crustal and upper mantle materials and stripping away of a thinned basaltic section by detachment faults. In the OCC model, serpentinization was localized to some peridotite sections and fault zones, potentially at odds with the analysis of *ten Brink et al.* [2002]; note that some workers argue that serpentinization should, in general, have a subdued effect on gravity anomalies [e.g., *Christensen*, 2004]. The result of this evolution was the consolidation of basaltic volcanic units to the deeper basins over thinner crust to the east, and predominantly gabbro-peridotite massifs to the west. According to our interpretation, the youngest (after the axial region) of the OCC-hanging wall pairs is ~50–75 km from the MCSC within ~10 Ma old crust, and the older pair developed ~120–170 km from the MCSC, ~20 Ma ago. Therefore, the OCCs developed episodically, but with the net effect that the MCSC has a long-term asymmetric seafloor spreading rate, also recognized in seafloor magnetic anomalies [*Rosencrantz et al.*, 1988; *Leroy et al.*, 2000].

[39] The aforementioned petrological, geochemical, and structural relationships in the MCSC lead us to favor the OCC model for MCSC spreading. However, it is worth considering some *inconsistencies* with the OCC model. Despite the abundance of alteration minerals in the ultramafic units, and though detachment faults would be an efficient way for the MCSC to exhume deeper materials, work to date has not recognized the *syntectonic* greenschist facies mineral assemblage in ultramafic rocks commonly associated with many other OCCs; for example, to date there are no reports of well-defined MCSC talc + tremolite ± serpentine rich shear zones such as found in OCC-bounding detachment faults elsewhere [*Boschi et al.*, 2006; *Escartín et al.*, 2003; *Schroeder and John*, 2004; *Karson et al.*, 2006]. Of the serpentinites sampled from the MCSC, orthopyroxene and spinel define

the foliations suggesting that they predate crustal deformation. Similarly, the proposed OCC surfaces are not as clearly and continuously corrugated as many other OCCs [*Cann et al.*, 1997; *MacLeod et al.*, 2009]. Earthquake focal mechanisms (Figure 1) and patterns in the bathymetric structure suggest that, at least locally, EW striking strike-slip faults cut across the OCCs, both near the MCSC transform boundaries and within the MCSC along the southern margin of Mount Dent [*Macdonald and Holcombe*, 1978]; though many OCCs occur along inside corners, such transcurrent faulting is not considered in OCC models. Last, the vent field atop Mount Dent may require an off-axis heat source perhaps signaling that an additional process, such as off-axis magmatic underplating, may be responsible for some of the distinctive bathymetric structure and hydrothermal alteration. Similar off-axis sulfide deposits and vent systems have been identified along the Mid-Atlantic Ridge [*Cherkashov et al.*, 2010].

[40] In contrast with possible alternative hypotheses, future work may strengthen the OCC model by finding highly strained schists and/or serpentinites and corrugations along well-defined detachment shear zones that bound Mount Dent and the other MCSC massifs. Strike-slip faults may not greatly affect the spreading-center processes and provide further fluid pathways to the off-axis hydrothermal system [e.g., *Hirose and Hayman*, 2008], and off-axis magmatism may be relatively insignificant. The final phases of exhumation and extension across the MCSC undoubtedly were accommodated by high-angle faults that cut any detachments, but this is consistent with the structural evolution proposed for other OCCs [e.g., *Karson et al.*, 2006]; such high-angle faults are a natural consequence of footwall exhumation (along with significant rotations) into the upper crust in many OCC models [e.g., *Schouten et al.*, 2010]. Last, barring future seismic imaging and petrological research, there is no reason to suspect that upper mantle and lower crustal materials exposed at the MCSC seafloor did not require several kilometers of exhumation accommodated by a detachment shear zone.

[41] Our model for the evolution of the Cayman trough envisions crustal thickness and seafloor depth variations as resulting through OCC development and associated crustal processes. Our model therefore contrasts with prevailing models for crustal thickness and axial depth variation that focus on the thermal structure of the adiabatic melting column, which is thought to be sensitive to spreading rates <20 mm/yr [*Reid and Jackson*, 1981; *Klein and Langmuir*, 1987; *White et al.*, 2001]. What is puzzling, though, is that according to our magnetic anomaly interpretation, the MCSC spreading rate has remained 15–20 mm/yr throughout its history, thought to favor a melt-poor regime that in turn is not generally expected to favor OCC development [*Buck et al.*, 2005; *Ito and Behn*, 2008; *Behn and Ito*, 2008]. Perhaps the MCSC is an example of the heterogeneous distribution of melts in an overall melt-poor environment [*Tucholke et al.*, 2008; *Olive et al.*, 2010]. Further research on the MCSC may find it a particularly advantageous site for an investigation of the relationship between OCCs and other MOR properties, given the difficulty in establishing such relationships along longer, more remote ultraslow ridges with inferred along-axis variations in mantle temperature [e.g., *Grindlay et al.*, 1998] and spreading obliquity [e.g., *Dick et al.*, 2003].

7. Conclusion

[42] Drawing on both previously published and unpublished bathymetric, geophysical, microstructural, petrological, and geochemical data, we advance an oceanic core complex (OCC) model for seafloor spreading at the ultraslow Mid-Cayman Spreading Center (MCSC). The model describes how (1) primitive liquids evolved between the upper mantle and base of the crust via crystal fractionation, the subsequent accumulation of near-liquidus phases in the gabbros, and generation of relatively homogenous MORB lavas, (2) gabbro and surrounding peridotite were exhumed along high-temperature shear zones before being altered at greenschist to amphibolite facies conditions with hydrothermal fluids that fed seafloor hydrothermal vents, and (3) the OCCs were finally uplifted and cut by high-angle faults resulting in a deep intraridge rift with volcanic sections in detachment fault contact with gabbro and peridotite. An OCC model for the MCSC and Cayman trough is significant because it provides a framework for the heterogeneous distribution of basalts, gabbros, and peridotites in a key ultraslow spreading environment. The model also explains patterns of axial depth and crustal thickness observed in both the spreading center and older regions of the Cayman trough. Ongoing seafloor spreading within the MCSC sets the physical, chemical, and thermal conditions for hydrothermal systems which feed vents within the axial and off-axis MCSC.

Acknowledgments

[43] Leroy and Mercier de Lépinay thank the CAYVIC crew and cruise participants. We thank Sharon Perez-Suarez for her geochemical study of the Cayman trough and Henry Dick for providing her with some of the gabbroic samples, access to the Woods Hole Oceanographic Institution ion microprobe, and his unpublished data. Perez-Suarez was partially supported by a Minority Research Training Award of the Woods Hole Oceanographic Institution and a Graduate Assistantship at the University of Florida. This paper was completed during the 2010 RRS James Cook cruise to the Cayman trough, and Grindlay and Hayman thank Doug Connelly, Bramley Murton, and Jon Copley for inviting them to participate. We thank Patty Ganey-Curry (UTIG) and Tim Le Bas (Southampton) for assistance with the aeromagnetic data set. We thank Andrew McCaig and an anonymous reviewer for helpful comments on the paper. This work was partly supported by a UTIG innovation and opportunity grant and the Caribbean Basins Tectonics and Hydrocarbon project. This is UTIG contribution 2305.

References

Baker, E., and C. German (2004), On the global distribution of mid-ocean ridge hydrothermal vent-fields, in *Mid-Ocean Ridges: Hydrothermal Interactions Between the Lithosphere and Oceans*, *Geophys. Monogr.*, vol. 148, edited by C. R. German, J. Lin, and L. M. Parson, pp. 245–266, AGU, Washington D. C.

Baker, E. T., Y. J. Chen, and J. P. Morgan (1996), The relationship between near-axis hydrothermal cooling and the spreading rate of mid-ocean ridges, *Earth Planet. Sci. Lett.*, *142*, 137–145, doi:10.1016/0012-821X(96)00097-0.

Baran, J. M., et al. (2009), Constraints on the mantle temperature gradient along the Southeast Indian Ridge from crustal structure and isostasy: Implications for the transition from axial high to an axial valley, *Geophys. J. Int.*, *179*, 144–153, doi:10.1111/j.1365-246X.2009.04300.x.

Behn, M. D., and G. Ito (2008), Magmatic and tectonic extension at mid-ocean ridges: 1. Controls on fault characteristics, *Geochem. Geophys. Geosyst.*, *9*, Q08O10, doi:10.1029/2008GC001965.

Blackman, D. K., B. Ildefonse, B. E. John, Y. Ohara, D. J. Miller, C. J. MacLeod, and the Expedition 304/305 Scientists (2006), *Proceedings of the Integrated Ocean Drilling Program*, vol. 304/305, Integrated Ocean Drill. Program, College Station, Tex., doi:10.2204/iodp.proc.304305.2006.

Boschi, C., G. L. Früh-Green, J. A. Karson, D. S. Kelley, and A. G. Delacour (2006), Mass transfer and fluid flow during detachment faulting and development of an oceanic core complex, Atlantis Massif (MAR 30°N), *Geochem. Geophys. Geosyst.*, *7*, Q01004, doi:10.1029/2005GC001074.

Bowin, C. (1968), Geophysical study of the Cayman trough, *J. Geophys. Res.*, *73*, 5159–5173, doi:10.1029/JB073i016p05159.

Buck, W. R., L. L. Lavier, and A. N. B. Poliakov (2005), Modes of faulting at mid-ocean ridges, *Nature*, *434*, 719–723, doi:10.1038/nature03358.

Cann, J. R., et al. (1997), Corrugated slip surfaces formed at ridge-transform intersections on the Mid-Atlantic Ridge, *Nature*, *385*, 329–332, doi:10.1038/385329a0.

Cannat, M., D. Sauter, V. Mendel, E. Ruellan, K. Okino, J. Escartin, V. Combier, and M. Baala (2006), Modes of seafloor generation at a melt-poor ultraslow-spreading ridge, *Geology*, *34*, 605–608, doi:10.1130/G22486.1.

Cannat, M., D. Sauter, A. Bezos, C. Meyzen, E. Humler, and M. Le Rigoleur (2008), Spreading rate, spreading obliquity, and melt supply at the ultraslow spreading Southwest Indian Ridge, *Geochem. Geophys. Geosyst.*, *9*, Q04002, doi:10.1029/2007GC001676.

CAYTROUGH (1979), Geological and geophysical investigation of the Mid-Cayman Rise Spreading Center: Initial results and observations, in *Deep Drilling Results in the Atlantic Ocean: Oceanic Crust*, *Maurice Ewing Ser.*, vol. 2, edited by M. Talwani, G. G. Harrison, and D. E. Hays, pp. 66–93, AGU, Washington, D. C.

Chen, Y. J. (1992), Oceanic crustal thickness versus spreading rate, *Geophys. Res. Lett.*, *19*, 753–756, doi:10.1029/92GL00161.

Cherkashov, G., et al. (2010), Seafloor massive sulfides from the northern equatorial Mid-Atlantic Ridge: New discoveries and perspectives, *Mar. Georesour. Geotechnol.*, *28*, 222–239, doi:10.1080/1064119X.2010.483308.

Christensen, N. (2004), Serpentinites, peridotites, and seismology, *Int. Geol. Rev.*, *46*, 795–816, doi:10.2747/0020-6814.46.9.795.

Cochran, J. R., G. J. Kurras, M. H. Edwards, and B. J. Coakley (2003), The Gakkel Ridge: Bathymetry, gravity anomalies, and crustal accretion at extremely slow spreading rates, *J. Geophys. Res.*, *108*(B2), 2116, doi:10.1029/2002JB001830.

Coogan, L. A., P. D. Kempton, A. D. Saunders, and M. J. Norry (2000), Melt aggregation within the crust beneath the Mid-Atlantic Ridge: Evidence from plagioclase and clinopyroxene major and trace element compositions, *Earth Planet. Sci. Lett.*, *176*, 245–257, doi:10.1016/S0012-821X(00)00006-6.

de Martin, B. J., R. A. R. Canales, J. P. Canales, and S. E. Humphris (2007), Kinematics and geometry of active detachment faulting beneath the Trans-Atlantic Geotraverse (TAG) hydrothermal field on the Mid-Atlantic Ridge, *Geology*, *35*, 711–714, doi:10.1130/G23718A.1.

DeMets, C., and M. Wiggins-Grandison (2007), Deformation of Jamaica and motion of the Gonave microplate from GPS and seismic data, *Geophys. J. Int.*, *168*, 362–378, doi:10.1111/j.1365-246X.2006.03236.x.

DeMets, C., et al. (2007), Present motion and deformation of the Caribbean plate: Constraints from new GPS geodetic measurements from Honduras and Nicaragua, *Spec. Pap. Geol. Soc. Am.*, *428*, 21–36.

Dick, H. J. B. (1989), Abyssal peridotites, very slow spreading ridges and ocean ridge magmatism, in *Magmatism in the Ocean Basins*, edited by A. D. Saunders and M. J. Norry, *Geol. Soc. Spec. Publ.*, *42*, 71–105.

Dick, J. B., et al. (2000), A long in situ section of the lower ocean crust: Results of ODP Leg 176 drilling at the Southwest Indian Ridge, *Earth Planet. Sci. Lett.*, *179*, 31–51, doi:10.1016/S0012-821X(00)00102-3.

Dick, H. J. B., J. Lin, and H. Schouten (2003), An ultraslow-spreading class of ocean ridge, *Nature*, *426*, 405–412, doi:10.1038/nature02128.

Dick, H. J. B., C. J. Lissenberg, and J. M. Warren (2010), Mantle melting, melt transport and delivery beneath a slow-spreading ridge: The paleo-MAR from 23°15′N to 23°45′N, *J. Petrol.*, *51*, 425–467, doi:10.1093/petrology/egp088.

Dillon, W. P., J. G. Vedder, and R. J. Graf (1972), Structural profile of northwest Caribbean, *Earth Planet. Sci. Lett.*, *17*, 175–180, doi:10.1016/0012-821X(72)90273-7.

Dixon, T. H., F. Farina, C. DeMets, P. Jansma, P. Mann, and E. Calais (1998), Relative motion between the Caribbean and North American plates and related plate boundary zone deformation from a decade of GPS observations, *J. Geophys. Res.*, *103*, 15,157–15,182, doi:10.1029/97JB03575.

Drouin, M., B. Ildefonse, and M. Godard (2010), A microstructural imprint of melt impregnation in slow spreading lithosphere: Olivine-rich troctolites from the Atlantis Massif, Mid-Atlantic Ridge, 30°N, IODP Hole U1309D, *Geochem. Geophys. Geosyst.*, *11*, Q06003, doi:10.1029/2009GC002995.

Eason, D., and J. M. Sinton (2006), Origin of high-Al N-MORB by fractional crystallization in the upper mantle beneath the Galápagos Spreading Center, *Earth Planet. Sci. Lett.*, *252*, 423–436, doi:10.1016/j.epsl.2006.09.048.

Edgar, N. T., W. P. Dillon, L. M. Parson, K. M. Scanlon, C. L. Jacobs, and T. L. Holcombe (1991), GLORIA Sidescan-Sonar Image and interpretation of the central Cayman trough, northwestern Caribbean Sea, *U.S. Geol. Surv. Misc. Field Stud. Map*, *MF-2083 A*, 3 sheets.

Elthon, D. (1987), Petrology of gabbroic rocks from the Mid-Cayman Rise Spreading Center, *J. Geophys. Res.*, *92*, 658–682, doi:10.1029/JB092iB01p00658.

Elthon, D., D. K. Ross, and J. K. Meen (1995), Compositional variations of basaltic glasses from the Mid-Cayman Rise Spreading Center, *J. Geophys. Res.*, *100*, 12,497–12,512, doi:10.1029/94JB02777.

Erickson, A. J., C. E. Helsey, and G. Simmons (1972), Heat flow and continuous seismic profiles in the Cayman trough and Yucatan Basin, *Geol. Soc. Am. Bull.*, *83*, 1241–1260, doi:10.1130/0016-7606(1972)83[1241:HFACSP]2.0.CO;2.

Escartín, J., P. A. Cowie, R. C. Searle, S. Allerton, N. C. Mitchell, C. J. MacLeod, and A. P. Slootweg (1999), Quantifying tectonic strain and magmatic accretion at a slow spreading ridge segment, Mid-Atlantic Ridge, 29°N, *J. Geophys. Res.*, *104*, 10,421–10,437, doi:10.1029/1998JB900097.

Escartín, J., C. Mével, C. J. MacLeod, and A. M. McCaig (2003), Constraints on deformation conditions and the origin of oceanic detachments: The Mid-Atlantic Ridge core complex at 15°45′N, *Geochem. Geophys. Geosyst.*, *4*(3), 1067, doi:10.1029/2002GC000472.

Escartín, J., D. K. Smith, J. Cann, H. Schouten, C. H. Langmuir, and S. Escrig (2008), Central role of detachment faults in accretion of slow-spreading oceanic lithosphere, *Nature*, *455*, 790–794, doi:10.1038/nature07333.

Ewing, J., J. Antoine, and M. Ewing (1960), Geophysical measurements in the western Caribbean Sea and in the Gulf of Mexico, *J. Geophys. Res.*, *65*, 4087–4126, doi:10.1029/JZ065i012p04087.

Fujiwara, T., and H. Fujimoto (1998), Seafloor geomagnetic vector anomaly of the intersection of the Mid-Atlantic Ridge and the Kane Transform Fault: Implications for magnetization of the oceanic crust, *J. Geophys. Res.*, *103*, 30,335–30,349, doi:10.1029/1998JB900015.

Gao, Y., et al. (2007), Trace element zoning in pyroxenes from ODP Hole 735B gabbros: Diffusive exchange or synkinematic crystal fractionation?, *Contrib. Mineral. Petrol.*, *153*, 429–442, doi:10.1007/s00410-006-0158-4.

Garcés, M., and J. S. Gee (2007), Paleomagnetic evidence of large footwall rotations associated with low-angle faults at the Mid-Atlantic Ridge, *Geology*, *35*, 279–282, doi:10.1130/G23165A.1.

German, C. R., et al. (2010), Diverse styles of submarine venting on the ultraslow spreading Mid-Cayman Rise, *Proc. Natl. Acad. Sci. U. S. A.*, *107*(32), 14,020–14,025, doi:10.1073/pnas.1009205107.

Godard, M., et al. (2009), Geochemistry of a long in-situ section of intrusive slow-spread oceanic lithosphere: Results from IODP Site U1309 (Atlantis Massif, 30N Mid-Atlantic Ridge), *Earth Planet. Sci. Lett.*, *279*, 110–122, doi:10.1016/j.epsl.2008.12.034.

Grimes, C. B., B. E. John, M. J. Cheadle, and J. L. Wooden (2008), Protracted construction of gabbroic crust at a slow spreading ridge: Constraints from $^{206}Pb/^{238}U$ zircon ages from Atlantis Massif and IODP Hole U1309D (30°N, MAR), *Geochem. Geophys. Geosyst.*, *9*, Q08012, doi:10.1029/2008GC002063.

Grindlay, N. R., J. A. Madsen, C. Rommevaux-Jestin, and J. Sclater (1998), A different pattern of ridge segmentation and mantle Bouguer gravity anomalies along the ultra-slow spreading Southwest Indian Ridge (15°30′E to 25°E), *Earth Planet. Sci. Lett.*, *161*, 243–253, doi:10.1016/S0012-821X(98)00154-X.

Harigane, Y., K. Michibayashi, and Y. Ohara (2008), Shearing within lower crust during progressive retrogression: Structural analysis of gabbroic rocks from the Godzilla Mullion, an oceanic core complex in the Parece Vela backarc basin, *Tectonophysics*, *457*, 183–196, doi:10.1016/j.tecto.2008.06.009.

Herzberg, C. (2004), Partial crystallization of mid-ocean ridge basalts in the crust and mantle, *J. Petrol.*, *45*, 2389–2405, doi:10.1093/petrology/egh040.

Hirose, T., and N. W. Hayman (2008), Structure, permeability, and strength of a fault zone in the footwall of an oceanic core complex, the central dome of the Atlantis Massif, Mid-Atlantic Ridge, 30N, *J. Struct. Geol.*, *30*(8), 1060–1071, doi:10.1016/j.jsg.2008.04.009.

Holcombe, T. L., and G. F. Sharman (1983), Post-Miocene Cayman trough evolution: A speculative model, *Geology*, *11*, 714–717, doi:10.1130/0091-7613(1983)11<714:PCTEAS>2.0.CO;2.

Ildefonse, B., D. K. Blackman, B. E. John, Y. Ohara, D. J. Miller, and C. J. MacLeod (2007), Oceanic core complexes and crustal accretion at slow-spreading ridges, *Geology*, *35*, 623–626, doi:10.1130/G23531A.1.

Ito, E., and A. T. Anderson (1983), Submarine metamorphism of gabbros from the Mid-Cayman Rise: Petrographic and mineralogic constraints on hydrothermal processes as slow-spreading centers, *Contrib. Mineral. Petrol.*, *82*, 371–388, doi:10.1007/BF00399714.

Ito, G., and M. D. Behn (2008), Magmatic and tectonic extension at mid-ocean ridges: 2. Origin of axial morphology, *Geochem. Geophys. Geosyst.*, *9*, Q09O12, doi:10.1029/2008GC001970.

Ito, E., and R. N. Clayton (1983), Submarine metamorphism of gabbros from the Mid-Cayman Rise: An oxygen isotopic study, *Geochim. Cosmochim. Acta*, *47*, 535–546, doi:10.1016/0016-7037(83)90276-4.

Jacobs, C. L., N. T. Edgar, L. M. Parson, W. P. Dillon, K. M. Scanlon, and T. L. Holcombe (1989), A revised bathymetry of the Mid-Cayman Rise and central Cayman trough using long-ranges side scan sonar, *Rep. 272*, 11 pp. and chart, Inst. of Oceanogr. Sci. Deacon Lab., Surrey, U. K.

John, B. E., D. A. Foster, J. M. Murphy, M. J. Cheadle, A. G. Baines, C. M. Fanning, and P. Copeland (2004), Determining the cooling history of in situ lower oceanic crust—Atlantis Bank, SW Indian Ridge, *Earth Planet. Sci. Lett.*, *222*, 145–160, doi:10.1016/j.epsl.2004.02.014.

Jordan, T. H. (1975), The present-day motions of the Caribbean plate, *J. Geophys. Res.*, *80*, 4433–4439, doi:10.1029/JB080i032p04433.

Karson, J. A. (1999), Geological investigation of a lineated massif at the Kane transform: Implications for oceanic core complexes, *Philos. Trans. R. Soc. London A*, *357*, 713–740, doi:10.1098/rsta.1999.0350.

Karson, J. A., and P. J. Fox (1986), Geological and geophysical investigation of the Mid-Cayman Spreading Center: Seismic velocity measurements and implications for the constitution of Layer 3, *Geophys. J. R. Astron. Soc.*, *85*, 389–411, doi:10.1111/j.1365-246X.1986.tb04520.x.

Karson, J. A., E. A. Williams, G. L. Früh-Green, D. S. Kelley, D. R. Yoerger, and M. Jakuba (2006), Detachment shear zone on the Atlantis Massif Core Complex, Mid-Atlantic Ridge 30°N, *Geochem. Geophys. Geosyst.*, *7*, Q06016, doi:10.1029/2005GC001109.

Klein, E. M., and C. H. Langmuir (1987), Global correlations of ocean ridge basalt chemistry with axial depth and crustal thickness, *J. Geophys. Res.*, *92*, 8089–8115, doi:10.1029/JB092iB08p08089.

Leroy, S., B. Mercier de Lepinay, A. Mauffret, and M. Pubellier (1996), Structure and tectonic evolution of the eastern Cayman trough (Caribbean Sea) from multichannel seismic data, *AAPG Bull.*, *80*, 222–247.

Leroy, S., A. Mauffret, P. Patriat, and B. Mercier de Lepinay (2000), An alternative interpretation of the Cayman trough evolution from a re-identification of magnetic anomalies, *Geophys. J. Int.*, *141*, 539–557, doi:10.1046/j.1365-246x.2000.00059.x.

Lissenberg, C. J., and H. J. B. Dick (2008), Melt-rock reaction in the lower oceanic crust and its implications for the genesis of mid-ocean ridge basalt, *Earth Planet. Sci. Lett.*, *271*, 311–325, doi:10.1016/j.epsl.2008.04.023.

Macdonald, K. C., and T. L. Holcombe (1978), Inversion of magnetic anomalies and sea-floor spreading in the Cayman trough, *Earth Planet. Sci. Lett.*, *40*, 407–414, doi:10.1016/0012-821X(78)90163-2.

Macdonald, K. C., S. P. Miller, S. P. Heustis, and F. N. Spiess (1980), Three-dimensional modeling of a magnetic reversal boundary from inversion of deep-tow measurements, *J. Geophys. Res.*, *85*, 3670–3680, doi:10.1029/JB085iB07p03670.

MacLeod, C. J., R. C. Searle, B. J. Murton, J. F. Casey, C. Mallows, S. C. Unsworth, K. L. Achenbach, and M. Harris (2009), Life cycle of oceanic core complexes, *Earth Planet. Sci. Lett.*, *287*, 333–344, doi:10.1016/j.epsl.2009.08.016.

Malcolm, F. L. (1981), Microstructures of the Cayman trough gabbros, *J. Geol.*, *89*, 675–688, doi:10.1086/628635.

Mann, P. (1999), Caribbean sedimentary basins: Classification and tectonic setting from Jurassic to present, in *Caribbean Basins, Sedimentary Basins of the World*, vol. 4, pp. 3–31, Elsevier, Amsterdam.

Mann, P. (2007), Overview of the tectonic history of northern Central America, *Spec. Pap. Geol. Soc. Am.*, *428*, 1–19.

McCaig, A. M., R. A. Cliff, J. Escartín, A. E. Fallick, and C. J. MacLeod (2007), Oceanic detachment faults focus very large volumes of black smoker fluids, *Geology*, *35*, 935–938, doi:10.1130/G23657A.1.

Michael, P. J., et al. (2003), Magmatic and amagmatic seafloor generation at the ultraslow-spreading Gakkel Ridge, Arctic Ocean, *Nature*, *423*, 956–961, doi:10.1038/nature01704.

Michibayashi, K., T. Hirose, T. Nozaka, Y. Harigane, J. Escartín, H. Delius, M. Linek, and Y. Ohara (2008), Hydration due to high-T brittle failure within in situ oceanic crust, 30°N Mid-Atlantic Ridge, *Earth Planet. Sci. Lett.*, *275*, 348–354, doi:10.1016/j.epsl.2008.08.033.

Miranda, E. A., and B. E. John (2010), Strain localization along the Atlantis Bank oceanic detachment fault system, Southwest Indian Ridge, *Geochem. Geophys. Geosyst.*, *11*, Q04002, doi:10.1029/2009GC002646.

Morris, A., J. S. Gee, N. Pressling, B. E. John, C. J. MacLeod, C. B. Grimes, and R. C. Searle (2009), Footwall rotation in an oceanic core complex quantified using reoriented Integrated Ocean Drilling Program core samples, *Earth Planet. Sci. Lett.*, *287*, 217–228, doi:10.1016/j.epsl.2009.08.007.

Muller, M. R., T. A. Minshull, and R. S. White (2000), Crustal structure of the Southwest Indian Ridge at the Atlantis II Fracture Zone, *J. Geophys. Res.*, *105*, 25,809–25,828, doi:10.1029/2000JB900262.

Murton, B. J., D. P. Connelly, J. T. Copley, K. L. Stansfield, and P. A. Tyler (2010), Hydrothermal vents at 5000 m on the Mid-Cayman Rise: The deepest and hottest hydrothermal systems yet discovered, Abstract OS33F-05 presented at 2010 Fall Meeting, AGU, San Francisco, Calif., 13–17 Dec.

Natland, J. H., and H. J. B. Dick (2001), Formation of the lower oceanic crust and the crystallization of gabbroic cumulates at a very slowly spreading ridge, *J. Volcanol. Geotherm. Res.*, *110*(3–4), 191–233, doi:10.1016/S0377-0273(01)00211-6.

Okino, K., D. Curewitz, M. Asada, K. Tamaki, P. Vogt, and K. Crane (2002), Preliminary analysis of the Knipovich Ridge segmentation: Influence of focused magmatism and ridge obliquity on an ultraslow spreading system, *Earth Planet. Sci. Lett.*, *202*, 275–288, doi:10.1016/S0012-821X(02)00790-2.

Olive, J. A., M. D. Behn, and B. E. Tucholke (2010), The structure of oceanic core complexes controlled by the depth distribution of magma emplacement, *Nat. Geosci.*, *3*(7), 491–495, doi:10.1038/ngeo888.

Parker, R. L., and S. P. Huestis (1974), The inversion of magnetic anomalies in the presence of topography, *J. Geophys. Res.*, *79*, 1587–1593, doi:10.1029/JB079i011p01587.

Perez-Suarez, S. D. (2001), *Petrology and Geochemistry of the Mid-Cayman Rise: An End-Member for the Lower Crust of a Mid-Ocean Ridge*, 123 pp., Univ. of Florida, Gainesville, Fla.

Perfit, M. R. (1977), Petrology and geochemistry of mafic rocks form the Cayman Trench: Evidence for spreading, *Geology*, *5*, 105–110, doi:10.1130/0091-7613(1977)5<105:PAGOMR>2.0.CO;2.

Perfit, M. R., and B. C. Heezen (1978), The geology and evolution of the Cayman Trench, *Geol. Soc. Am. Bull.*, *89*, 1155–1174, doi:10.1130/0016-7606(1978)89<1155:TGAEOT>2.0.CO;2.

Reid, I., and H. R. Jackson (1981), Ocean spreading rate and crustal thickness, *Mar. Geophys. Res.*, *5*, 165–172.

Rosencrantz, E. (1995), Opening of the Cayman trough and the evolution of the northern Caribbean plate boundary, *Geol. Soc. Am. Abstr. Programs*, *27*, 153.

Rosencrantz, E., and P. Mann (1991), SeaMARC II mapping of transform faults in the Cayman trough, Caribbean Sea, *Geology*, *19*, 690–693, doi:10.1130/0091-7613(1991)019<0690:SIMOTF>2.3.CO;2.

Rosencrantz, E., R. I. Malcom, and J. G. Sclater (1988), Age and spreading history of the Cayman trough as determined from depth, heat flow, and magnetic anomalies, *J. Geophys. Res.*, *93*, 2141–2157, doi:10.1029/JB093iB03p02141.

Ruellan, E., B. Mercier de Lepinay, M.-O. Beslier, M. Sosson, C. Monnier, S. Leroy, D. Rowe, and G. Cruz Calderon

(2003), Morphology and tectonics of the Mid-Cayman Spreading Center (CAYVIC cruise), *Geophys. Res. Abstr.*, *5*, 12,580.

Sauter, D., M. Cannat, and V. Mendel (2008), Magnetization of 0–26.5 Ma seafloor at the ultraslow spreading Southwest Indian Ridge, 61°–67°E, *Geochem. Geophys. Geosyst.*, *9*, Q04023, doi:10.1029/2007GC001764.

Schouten, H., D. K. Smith, J. R. Cann, and J. Escartín (2010), Tectonic versus magmatic extension in the presence of core complexes at slow-spreading ridges from a visualization of faulted seafloor topography, *Geology*, *38*, 615–618, doi:10.1130/G30803.1.

Schroeder, T., and B. E. John (2004), Strain localization on an oceanic detachment fault system, Atlantis Massif, 30°N, Mid-Atlantic Ridge, *Geochem. Geophys. Geosyst.*, *5*, Q11007, doi:10.1029/2004GC000728.

Smith, D. K., J. R. Cann, and J. Escartín (2006), Widespread active detachment faulting and core complex formation near 13°N on the Mid-Atlantic Ridge, *Nature*, *442*, 440–443, doi:10.1038/nature04950.

Smith, D. K., J. Escartín, H. Schouten, and J. R. Cann (2008), Fault rotation and core complex formation: Significant processes in seafloor formation at slow-spreading mid-ocean ridges (Mid-Atlantic Ridge, 13°–15°N), *Geochem. Geophys. Geosyst.*, *9*, Q03003, doi:10.1029/2007GC001699.

Standish, J. J., H. J. B. Dick, P. J. Michael, W. G. Melson, and T. O'Hearn (2008), MORB generation beneath the ultraslow spreading Southwest Indian Ridge (9°–25°E): Major element chemistry and the importance of process versus source, *Geochem. Geophys. Geosyst.*, *9*, Q05004, doi:10.1029/2008GC001959.

Stroup, J. B., and P. J. Fox (1981), Geologic investigations in the Cayman trough: Evidence for thin crust along the Mid-Cayman Rise, *J. Geol.*, *89*, 395–420, doi:10.1086/628605.

Suhr, G., E. Hellebrand, K. Johnson, and D. Brunelli (2008a), Stacked gabbro units and intervening mantle: A detailed look at a section of IODP Leg 305, Hole U1309D, *Geochem. Geophys. Geosyst.*, *9*, Q10007, doi:10.1029/2008GC002012.

Suhr, G., P. Kelemen, and H. Paulick (2008b), Microstructures in Hole 1274A peridotites, ODP Leg 209, Mid-Atlantic Ridge: Tracking the fate of melts percolating in peridotite as the lithosphere is intercepted, *Geochem. Geophys. Geosyst.*, *9*, Q03012, doi:10.1029/2007GC001726.

Sun, S. S., and W. F. McDonough (1989), Chemical and isotopic systematics of oceanic basalts: Implications for mantle composition and processes, in *Magmatism in the Ocean Basins*, edited by A. D. Saunders and M. J. Norry, *Geol. Soc. Spec. Publ.*, *42*, 313–345.

Molnar, P., and L. R. Sykes (1969), Tectonics of the Caribbean and Middle America regions from focal mechanisms and seismicity, *Geol. Soc. Am. Bull.*, *80*, 1639–1684, doi:10.1130/0016-7606(1969)80[1639:TOTCAM]2.0.CO;2.

ten Brink, U., D. Coleman, and W. P. Dillon (2002), The nature of the crust under Cayman trough from gravity, *Mar. Pet. Geol.*, *19*, 971–987, doi:10.1016/S0264-8172(02)00132-0.

Thompson, G., W. B. Bryan, and W. G. Melson (1980), Geological and geophysical investigation of the Mid-Cayman Rise Spreading Center: Geochemical variation and petrogenesis of basalt glasses, *J. Geol.*, *88*, 41–55, doi:10.1086/628472.

Tucholke, B. E., J. Lin, and M. C. Kleinrock (1998), Megamullions and mullion structure defining oceanic metamorphic core complexes on the Mid-Atlantic Ridge, *J. Geophys. Res.*, *103*, 9857–9866, doi:10.1029/98JB00167.

Tucholke, B. E., M. D. Behn, W. R. Buck, and J. Lin (2008), Role of melt supply in oceanic detachment faulting and formation of megamullions, *Geology*, *36*, 455–458, doi:10.1130/G24639A.1.

Tyler, P. A., C. R. German, E. Ramirez-Llodra, and C. L. Van Dover (2002), ChEss: Understanding the biogeography of chemosynthetic ecosystems, *Oceanol. Acta*, *25*, 227–241, doi:10.1016/S0399-1784(02)01202-1.

Van Dover, C. L., C. R. German, K. G. Speer, L. M. Parson, and R. C. Vrijenhoek (2002), Evolution and biogeography of deep-sea vent and seep invertebrates, *Science*, *295*(5558), 1253–1257, doi:10.1126/science.1067361.

Warren, J. M., and N. Shimizu (2010), Cryptic variations in abyssal peridotite compositions: Evidence for shallow-level melt infiltration in the oceanic lithosphere, *J. Petrol.*, *51*, 395–423, doi:10.1093/petrology/egp096.

White, R. S., T. A. Minshull, M. J. Bickle, and C. J. Robinson (2001), Melt generation at very slow-spreading ocean ridges: Constraints from geochemical and geophysical data, *J. Petrol.*, *42*, 1171–1196, doi:10.1093/petrology/42.6.1171.